

Signal Detection and Channel Estimation in OTFS



Ashwitha NAIKOTI, Ananthanarayanan CHOCKALINGAM

(Department of ECE, Indian Institute of Science, Bangalore 560012, India)

Abstract: Orthogonal time frequency space (OTFS) modulation is a recently proposed modulation scheme that exhibits robust performance in high-Doppler environments. It is a two-dimensional modulation scheme where information symbols are multiplexed in the delay-Doppler (DD) domain. Also, the channel is viewed in the DD domain where the channel response is sparse and time-invariant for a long time. This simplifies channel estimation in the DD domain. This paper presents an overview of the state-of-the-art approaches in OTFS signal detection and DD channel estimation. We classify the signal detection approaches into three categories, namely, low-complexity linear detection, approximate maximum a posteriori (MAP) detection, and deep neural network (DNN) based detection. Similarly, we classify the DD channel estimation approaches into three categories, namely, separate pilot approach, embedded pilot approach, and superimposed pilot approach. We compile and present an overview of some of the key algorithms under these categories and illustrate their performance and complexity attributes.

Keywords: OTFS modulation; delay-Doppler domain; high-Doppler channels; signal detection; channel estimation

DOI: 10.12142/ZTECOM.202104003

<https://kns.cnki.net/kcms/detail/34.1294.TN.20211207.1647.002.html>, published online December 8, 2021

Manuscript received: 2021-10-18

Citation (IEEE Format): A. Naikoti and A. Chockalingam, "Signal detection and channel estimation in OTFS," *ZTE Communications*, vol. 19, no. 4, pp. 16 - 33, Dec. 2021. doi: 10.12142/ZTECOM.202104003.

1 Introduction

Next-generation wireless systems are expected to support a variety of use cases with a wide range of performance requirements. Interest in high-mobility use cases involving high-speed trains, unmanned vehicles/cars, drones, aeroplanes, etc., is on the rise. Also, in order to meet the growing bandwidth requirement, a wireless spectrum in the mmWave frequency band is preferred. Communication in such high-mobility and/or high carrier frequency scenarios has to deal with high Doppler shifts which are common in such environments. Orthogonal frequency division multiplexing (OFDM) is a widely used communication waveform in the current generation of wireless systems. De-

spite its popularity and adoption in current standards, OFDM suffers from severe performance degradation in high-Doppler scenarios. This is because of the increased loss of orthogonality among subcarriers and the resulting inter-carrier interference (ICI).

Orthogonal time frequency space (OTFS) modulation is a recently introduced 2-dimensional (2D) modulation^[1]. There has been growing interest in this modulation recently, because of its superior performance compared with OFDM in high-Doppler environments^[2-6]. In OTFS modulation, information symbols are multiplexed in the delay-Doppler (DD) domain. The symbols in the DD domain are converted to the time domain and transmitted. At the receiver, the received

signal in the time domain is converted back to the DD domain where the information symbols are recovered. The DD domain to time domain conversion and vice versa can be done using two approaches. In the first approach, symbols from the DD domain are mapped to the time domain in two steps: DD to time-frequency (TF) domain conversion using inverse symplectic finite Fourier transform (ISFFT), followed by the TF domain to time domain conversion using Heisenberg transform^[1]. The corresponding inverse transforms map the received time-domain signal to the TF domain and then to the DD domain (Wigner transform followed by SFFT). The second approach is a direct one-step approach, where DD domain to time domain mapping is done using inverse Zak transform^[7]. At the receiver, the Zak transform maps the signal from the time domain directly to the DD domain. While the first approach has been adopted in most of the studies reported in the literature so far, the second approach is also gaining popularity. While the first approach can be implemented as an overlay on existing TF modulation schemes (such as OFDM), the second approach has the benefit of reduced implementation complexity.

Since the introduction of OTFS in 2017, there has been a spurt of research activities in OTFS leading to an increasing volume of publications on OTFS^[5-51]. Some of the key areas of focus in these works include DD signal representation in OTFS, input-output relation in the DD domain in the form of a linear vector channel model, framework for DD signal processing, signal detection algorithms, techniques for DD channel estimation, characterization of the peak-to-average power ratio (PAPR), the effect of practical pulse shapes, diversity analysis of OTFS, the effect of oscillator phase noise and IQ imbalance, multi-antenna OTFS, space-time coding and precoding in OTFS, multiuser OTFS on the uplink and downlink, etc. Recognizing that efficient signal detection and channel estimation techniques are crucial for the successful realization of OTFS systems in practice, we focus on these two key receiver functions in this paper.

We classify the OTFS signal detection approaches into three broad categories. The first is the linear detection approach, where the focus is on exploiting the structure inherent in the effective channel matrix for reducing complexity. The second approach is based on approximations to maximum a posteriori (MAP) detection, which aim near-optimal performance at reduced complexity. The last one is a recent approach involving deep neural networks (DNN). We highlight some of the algorithms in these categories reported in the literature. In highlighting various detection algorithms, perfect DD channel knowledge will be assumed at the receiver.

Similarly, we classify the DD channel estimation approaches into three categories. In the first approach, separate pilot frames are employed for DD channel estimation. The channel estimates obtained during the pilot frames are used for detec-

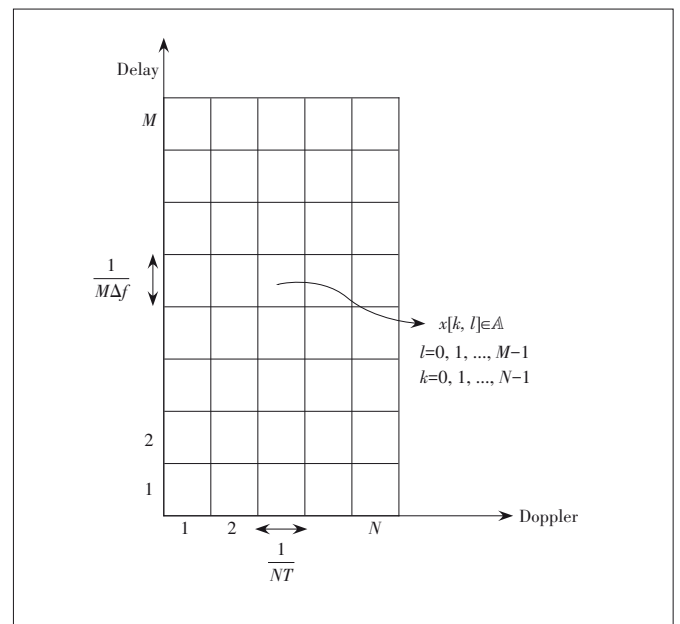
tion during data frames. The second approach involves embedding both pilot and data symbols in a frame. This further improves the throughput but the interference between pilot and data symbols needs to be taken into account by way of providing guard symbols around pilot symbols and/or interference cancellation. The last approach is the superimposed pilot approach, where pilot symbols are superimposed on data symbols. This further increases the throughput while demanding sophisticated signal processing (e. g., interference cancellation) to perform joint channel estimation and detection. We present algorithms reported in the literature under these categories.

The rest of this paper is organized as follows. Section 2 introduces the OTFS system model. Section 3 presents the state-of-the-art approaches and algorithms for OTFS signal detection. Section 4 presents the approaches and algorithms for DD channel estimation. Section 5 provides the conclusions.

2 OTFS Modulation and System Model

2.1 OTFS Modulation

In OTFS modulation, MN information symbols are multiplexed onto an $N \times M$ DD grid, where N is the number of Doppler bins and M is the number of delay bins, as shown in Fig. 1. The information symbols, denoted by $x[k, l]$, $k = 0, \dots, N-1$, $l = 0, \dots, M-1$, come from a modulation alphabet \mathbb{A} (e.g., QAM/PSK). The NM symbols are transmitted over a time duration of NT , occupying a bandwidth of $M\Delta f$, where $\Delta f = 1/T$. The Doppler resolution is $\frac{1}{NT}$ and the delay resolu-



▲ Figure 1. Multiplexing in delay-Doppler grid

tion is $\frac{1}{M\Delta f}$.

The symbols in the DD grid are mapped to a time-domain signal $x(t)$ for transmission. This can be done in two ways as shown in Fig. 2. In a two-step approach, the DD signal is first mapped to a time-frequency (TF) signal which is then mapped to a time-domain signal. The DD-to-TF domain mapping is done using ISFFT and the TF-to-time domain mapping is done using Heisenberg transform. In a one-step approach, the DD signal is directly mapped to a time-domain signal using inverse Zak transform. The corresponding inverse transforms are used at the receiver to demap the received time-domain signal to the DD domain. In this paper, we adopt the two-step approach which has been widely followed in the literature so far.

2.2 OTFS System Model

In this subsection, we present the OTFS system model for the two-step approach of DD-to-time domain conversion, as shown in Fig. 2(a). The symbols $x[k, l]$ in the DD domain are mapped to the TF domain using ISFFT, as

$$X[n, m] = \frac{1}{MN} \sum_{k=0}^{N-1} \sum_{l=0}^{M-1} x[k, l] e^{j2\pi\left(\frac{nk}{N} - \frac{ml}{M}\right)}. \quad (1)$$

This TF signal is transformed into a time-domain signal using Heisenberg transform, as

$$x(t) = \sum_{n=0}^{N-1} \sum_{m=0}^{M-1} X[n, m] g_{tx}(t - nT) e^{j2\pi m\Delta f(t - nT)}, \quad (2)$$

where $g_{tx}(t)$ defines the transmit pulse shape. The transmitted signal is passed through the channel whose response in the DD domain is given by

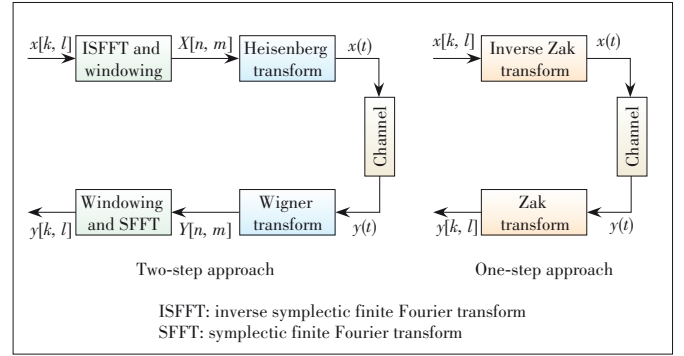
$$h(\tau, \nu) = \sum_{i=1}^P h_i \delta(\tau - \tau_i) \delta(\nu - \nu_i), \quad (3)$$

where h_i , τ_i , and ν_i are the channel gain, delay, and Doppler shift associated with the i -th path, respectively, and P is the number of resolvable paths in the DD domain.

The received time domain signal $y(t)$ at the receiver is given by

$$y(t) = \int_{\nu} \int_{\tau} h(\tau, \nu) x(t - \tau) e^{j2\pi\nu(t - \tau)} d\tau d\nu + v(t), \quad (4)$$

where $v(t)$ is the additive white Gaussian noise. Wigner transform is applied to $y(t)$ to transform it into a TF domain signal, as



▲ Figure 2. Orthogonal time frequency space (OTFS) modulation scheme

$$Y[n, m] = A_{g_{rx}, y}(t, f) \Big|_{t = nT, f = m\Delta f},$$

$$A_{g_{rx}, y}(t, f) = \int g_{rx}^*(t' - t) y(t) e^{-j2\pi f(t' - t)} dt', \quad (5)$$

where $g_{rx}(t)$ defines the receive pulse shape. If $g_{rx}(t)$ and $g_{tx}(t)$ satisfy the biorthogonality condition, the input-output relation in the TF domain is given by Ref. [11]:

$$Y[n, m] = H[n, m] X[n, m] + V[n, m], \quad (6)$$

where $V[n, m]$ is noise in TF domain and $H[n, m]$ is

$$H[n, m] = \int_{\tau} \int_{\nu} h(\tau, \nu) e^{j2\pi\nu nT} e^{-j2\pi(m + \nu\Delta f)\tau} d\nu d\tau. \quad (7)$$

The TF signal $Y[n, m]$ is transformed to the DD domain signal $y[k, l]$ using SFFT, as

$$y[k, l] = \sum_{n=0}^{N-1} \sum_{m=0}^{M-1} Y[n, m] e^{-j2\pi\left(\frac{nk}{N} - \frac{ml}{M}\right)}. \quad (8)$$

The above DD domain signal at the output of the SFFT can be derived to be of the form¹

$$y[k, l] = \sum_{i=1}^P h'_i x \left[\left(k - \beta_i \right)_N, \left(l - \alpha_i \right)_M \right] + v[k, l], \quad (9)$$

where $h'_i = h_i e^{-j2\pi\nu_i\tau_i}$, h_i s are i. i. d and are distributed as $\mathcal{CN}(0, 1/P)$ with uniform scattering profile, α_i and β_i are integers² corresponding to indices of delay and Doppler, respectively, for the i -th path, i.e., $\tau_i \triangleq \frac{\alpha_i}{M\Delta f}$ and $\nu_i \triangleq \frac{\beta_i}{NT}$, and $v[k, l]$ is the additive white Gaussian noise. By vectorizing the input-output relation in Eq. (9), we can write^[11]

$$\mathbf{y} = \mathbf{H}\mathbf{x} + \mathbf{v}, \quad (10)$$

where $\mathbf{x}, \mathbf{y}, \mathbf{v} \in \mathcal{C}^{MN \times 1}$, the $(k + Nl)$ -th entry of $\mathbf{x}, \mathbf{x}_{k + Nl} =$

1. Refer to Ref. [11] for the detailed derivation.

2. For the purpose of exposition of detection and channel estimation algorithms, integer Dopplers are considered in this paper. Refer to Ref. [11] for a similar system model for fractional Dopplers. Also, refer to Ref. [13] for the MIMO-OTFS system model.

$x[k, l], k = 0, \dots, N - 1, l = 0, \dots, M - 1$ and $x[k, l] \in \mathbb{A}$. Similarly, $y_{k+Ml} = y[k, l]$ and $v_{k+Ml} = v[k, l], k = 0, \dots, N - 1, l = 0, \dots, M - 1$, and $\mathbf{H} \in \mathcal{C}^{MN \times MN}$ is the effective channel matrix, whose j -th row ($j = k + Ml$), denoted by $\mathbf{H}[j]$, is given by $\mathbf{H}[j] = [\hat{h}((k-0)_N, (l-0)_M) \hat{h}((k-1)_N, (l-0)_M) \dots \hat{h}((k-N-1)_N, (l-M-1)_M)]$, where $\hat{h}(k, l)$ denotes the (k, l) -th element of the $N \times M$ DD channel matrix, given by

$$\hat{h}(k, l) = \begin{cases} h'_i, & \text{if } k = \beta_i, l = \alpha_i, i \in \{1, 2, \dots, P\} \\ 0, & \text{otherwise} \end{cases}. \quad (11)$$

It can be seen from the above that the effective channel matrix \mathbf{H} has only P non-zero entries in each row and column, i.e., there are only MNP non-zero elements in \mathbf{H} . The linear vector channel model in Eq. (10) is used for signal detection/equalization and channel estimation in OTFS.

3 OTFS Signal Detection

In this section, we present some of the signal detection algorithms proposed in the literature for OTFS modulation. Based on the approaches used, these algorithms are categorized into three groups, namely, 1) low-complexity linear detection, 2) approximate MAP detection, and 3) neural networks based detection, as shown in Fig. 3. We present algorithms under these categories in the following subsections, assuming perfect knowledge of the DD channel matrix. Later, in Section 4, we will present techniques/algorithms to estimate the channel matrix.

3.1 Low-Complexity Linear Detection

Linear equalizers detect the transmitted symbols by applying a linear transformation to the received vector \mathbf{y} followed by mapping to a symbol in the modulation alphabet \mathbb{A} which is closest in terms of euclidean distance. The linear transformation matrix is represented by \mathbf{G} and the mapping function is represented by $f(\cdot)$. Therefore, the estimate of the transmit vector \mathbf{x} is given by

$$\hat{\mathbf{x}} = f(\mathbf{G}\mathbf{y}). \quad (12)$$

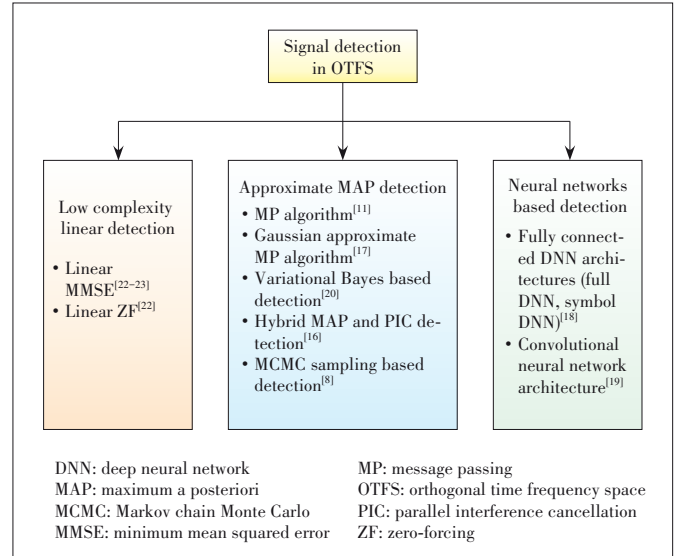
The transformation matrix for linear minimum mean squared error (LMMSE) equalization is given by

$$\mathbf{G}_{\text{lmmse}} = (\mathbf{H}^H \mathbf{H} + \sigma^2 \mathbf{I})^{-1} \mathbf{H}^H, \quad (13)$$

where σ^2 is the noise variance and the transformation matrix for zero-forcing (ZF) equalization is given by

$$\mathbf{G}_{\text{zf}} = (\mathbf{H}^H \mathbf{H})^{-1} \mathbf{H}^H. \quad (14)$$

These equalizers in the case of OTFS have a computation



▲ Figure 3. Signal detection approaches in OTFS

complexity of $\mathcal{O}(M^3 N^3)$. However, the structure of the channel matrix in the DD domain can be exploited to reduce the complexity of these operations^[22-23].

3.1.1 Low-Complexity LMMSE Equalization

In the low-complexity linear minimum mean square error (LMMSE) equalization^[22], the channel matrix \mathbf{H} in Eq. (10) has a block circulant structure with M circulant blocks denoted by \mathbf{A}_i ($i = 0, 1, \dots, M - 1$) of size $N \times N$. Using this property of the channel matrix, a low-complexity algorithm for implementing LMMSE equalization has been proposed in Ref. [22]. Let $\mathcal{C}_{M,N}$ denote the class of such block circulant matrices. These matrices have the following exploitable properties.

- Any matrix $\mathbf{H} \in \mathcal{C}_{M,N}$ can be unitarily diagonalizable as

$$\mathbf{H} = (\mathbf{F}_M \otimes \mathbf{F}_N)^H \mathbf{\Lambda} (\mathbf{F}_M \otimes \mathbf{F}_N), \quad (15)$$

where $\mathbf{\Lambda} = \text{diag}\{\lambda_1, \lambda_2, \dots, \lambda_{MN}\}$ such that λ_i is the i -th eigenvalue of \mathbf{H} , \mathbf{F}_M is the DFT matrix of size M , and \otimes is the Kronecker product operator.

- The matrix $\mathbf{\Lambda}$ can be written as

$$\mathbf{\Lambda} = \sum_{i=0}^{M-1} \mathbf{\Omega}_M^i \otimes \mathbf{A}_i, \quad (16)$$

where $\mathbf{\Omega}_M = \text{diag}\{1, \omega, \dots, \omega^{M-1}\}$ and $\omega = e^{j2\pi/M}$. \mathbf{A}_i is $N \times N$ diagonal matrix with eigenvalues of $N \times N$ circulant block \mathbf{A}_i on the diagonal.

For $\mathbf{A}, \mathbf{B} \in \mathcal{C}_{M,N}$, the matrices $\mathbf{A}^T, \mathbf{A}^H, \mathbf{AB} = \mathbf{BA}$, $c_1 \mathbf{A} + c_2 \mathbf{B}$, $\sum_{r=0}^{R-1} c_r \mathbf{A}_r$ (c_r are all scalars) and \mathbf{A}^{-1} (if exists) are also block circulant and belong to $\mathcal{C}_{M,N}$.

As $\mathbf{H} \in \mathcal{C}_{M,N}$, using the above properties, we have the LMMSE transformation matrix $\mathbf{G}_{\text{lmmse}} \in \mathcal{C}_{M,N}$. Thus, by substituting Eq. (15) in Eq. (13), we get

$$\mathbf{G}_{\text{lmmse}} = (\mathbf{F}_M \otimes \mathbf{F}_N)^H \boldsymbol{\Psi} (\mathbf{F}_M \otimes \mathbf{F}_N), \quad (17)$$

where $\boldsymbol{\Psi}$ is a diagonal matrix containing the eigenvalues of $\mathbf{G}_{\text{lmmse}}$, given by

$$\boldsymbol{\Psi} = (\mathbf{A}^* \mathbf{A} + \sigma^2 \mathbf{I})^{-1} \mathbf{A}^*, \quad (18)$$

where $\boldsymbol{\Psi}_i = \frac{\lambda_i^*}{|\lambda_i|^2 + \sigma^2}$, $i = 1, 2, \dots, MN$. To reduce the complexity of computing $(\mathbf{F}_M \otimes \mathbf{F}_N) \mathbf{y}$, write \mathbf{y} as an $N \times M$ matrix \mathbf{Y} such that $\text{vec}(\mathbf{Y}) = \mathbf{y}$. This gives

$$\mathbf{z} = (\mathbf{F}_M \otimes \mathbf{F}_N) \mathbf{y} = \text{vec}(\mathbf{F}_N \mathbf{Y} \mathbf{F}_M). \quad (19)$$

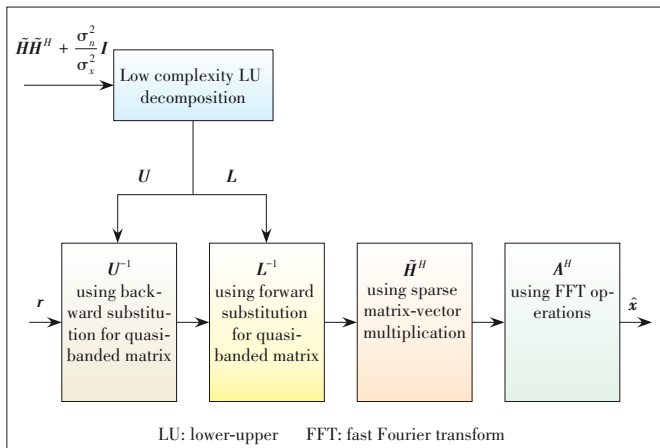
Now, compute $\mathbf{q} = \boldsymbol{\Psi} \mathbf{z}$ and write \mathbf{q} as a $N \times M$ matrix \mathbf{Q} such that $\text{vec}(\mathbf{Q}) = \mathbf{q}$. Finally, compute the estimated \mathbf{x} as

$$\hat{\mathbf{x}} = \mathbf{G}_{\text{lmmse}} \mathbf{y} = \text{vec}(\mathbf{F}_N^H \mathbf{Q} \mathbf{F}_M), \quad (20)$$

which gives the exact LMMSE solution at a much less computational complexity. The complexity of computing \mathbf{z} involving N -point DFT and M -point IDFT operations is $\mathcal{O}(MN \log MN)$ and the complexity of computing \mathbf{q} is $\mathcal{O}(MN)$. Again, the computation of $\hat{\mathbf{x}}$ involves N -point IDFT and M -point DFT operations with complexity $\mathcal{O}(MN \log MN)$. Therefore, the overall complexity is $\mathcal{O}(2MN \log MN + MN)$ which is much small compared to the $\mathcal{O}(M^3 N^3)$ complexity of conventional LMMSE detection using matrix inversion.

3.1.2 Low-Complexity LMMSE Equalization

As shown in Fig. 4, a low-complexity LMMSE equalization method that takes advantage of the sparse and quasi-banded nature of the OTFS demodulation matrices has been pro-



▲ Figure 4. Low complexity linear minimum mean squared error (LMMSE) equalization^[23]

posed in Ref. [23]. Here, a different representation of the system is used. The transmit vector \mathbf{x} in the DD domain is written as an $M \times N$ matrix \mathbf{X} such that $\text{vec}(\mathbf{X}) = \mathbf{x}$. Assume that $E[x(k, l) x^*(k', l')] = \sigma_x^2 \delta(k - k', l - l')$. Using this representation, we obtain vector \mathbf{s} as

$$\mathbf{s} = \text{vec}(\mathbf{X} \mathbf{F}_N^H). \quad (21)$$

This vector \mathbf{s} can also be written in the form $\mathbf{s} = \mathbf{A} \mathbf{x}$, where $\mathbf{A} = \mathbf{F}_N^H \otimes \mathbf{I}_M$ is a unitary matrix. The received vector \mathbf{r} at the receiver is given by

$$\mathbf{r} = \tilde{\mathbf{H}} \mathbf{s} + \mathbf{n} = \tilde{\mathbf{H}} \mathbf{A} \mathbf{x} + \mathbf{n}, \quad (22)$$

where $\tilde{\mathbf{H}} = \sum_{i=1}^P h_i \mathbf{\Pi}^{\alpha_i} \Delta^{\beta_i}$, $\mathbf{\Pi} = \text{circ}\{[010\dots 0]_{MN \times 1}^T\}$ is a circulant delay matrix, $\Delta = \text{diag}\left(1, e^{j2\pi \frac{1}{MN}}, \dots, e^{j2\pi \frac{MN-1}{MN}}\right)$ is a diagonal Doppler matrix, and \mathbf{n} is i.i.d Gaussian noise vector with variance σ_n^2 . The detected symbol vector for this system model in Eq. (22) using LMMSE equalization is given by

$$\hat{\mathbf{x}} = (\tilde{\mathbf{H}} \mathbf{A})^H \left[(\tilde{\mathbf{H}} \mathbf{A}) (\tilde{\mathbf{H}} \mathbf{A})^H + \frac{\sigma_n^2}{\sigma_x^2} \mathbf{I} \right]^{-1} \mathbf{r}. \quad (23)$$

Due to the unitary nature of \mathbf{A} , the above equation reduces to

$$\hat{\mathbf{x}} = \mathbf{A}^H \underbrace{\tilde{\mathbf{H}}^H \left[\tilde{\mathbf{H}} \tilde{\mathbf{H}}^H + \frac{\sigma_n^2}{\sigma_x^2} \mathbf{I} \right]^{-1}}_{\mathbf{H}_{eq}} \mathbf{r}. \quad (24)$$

This detected vector $\hat{\mathbf{x}}$ is obtained in two steps. The first step involves a calculation of $\tilde{\mathbf{r}} = \mathbf{H}_{eq} \mathbf{r}$ and the second step involves the matched filter operation $\mathbf{A}^H \tilde{\mathbf{r}}$ to get $\hat{\mathbf{x}}$. Most complexity is in the first step as it involves an inverse of $\boldsymbol{\Psi} = \left[\tilde{\mathbf{H}} \tilde{\mathbf{H}}^H + \frac{\sigma_n^2}{\sigma_x^2} \mathbf{I} \right]$ to obtain \mathbf{H}_{eq} . This complexity is reduced by using a low-complexity LU decomposition of $\boldsymbol{\Psi}$ ^[23]. With LU decomposition of $\boldsymbol{\Psi}$, we can write Eq. (24) as

$$\hat{\mathbf{x}} = \mathbf{A}^H \tilde{\mathbf{H}}^H \underbrace{\mathbf{U}^{-1} \mathbf{L}^{-1}}_{\mathbf{r}_2} \mathbf{r}. \quad (25)$$

The computational complexity can be further reduced by using the quasi-banded nature of lower triangular matrix \mathbf{L} and upper triangular matrix \mathbf{U} . In Eq. (25), \mathbf{r}_1 is computed using the forward substitution method for quasi-banded lower triangular matrix and \mathbf{r}_2 is computed using backward substitution method for quasi-banded upper triangular matrix. The final computation of $\hat{\mathbf{x}} = \mathbf{A}^H \tilde{\mathbf{H}}^H \mathbf{r}_2$ is done by first obtaining $\tilde{\mathbf{r}} = \tilde{\mathbf{H}}^H \mathbf{r}_2$. This vector $\tilde{\mathbf{r}}$ is arranged in an $M \times N$ matrix as

$$\hat{\mathbf{Y}} = \begin{bmatrix} \tilde{r}(0) & \tilde{r}(M) & \cdots & \tilde{r}(MN - N) \\ \tilde{r}(1) & \tilde{r}(M + 1) & \cdots & \tilde{r}(MN - N + 1) \\ \vdots & \vdots & \ddots & \vdots \\ \tilde{r}(M - 1) & \tilde{r}(2M - 1) & \cdots & \tilde{r}(MN - 1) \end{bmatrix}. \quad (26)$$

Using the matrix $\hat{\mathbf{Y}}$, $\hat{\mathbf{x}}$ is obtained using DFT operation as

$$\hat{\mathbf{x}} = \text{vec}(\hat{\mathbf{Y}}\mathbf{F}_N). \quad (27)$$

The main reduction in the complexity is in the computation of \tilde{r} . All the steps involved in obtaining r_2 together have a complexity of $\mathcal{O}(MN)$ and the final computation in Eq. (27) to obtain $\hat{\mathbf{x}}$ has a complexity of $\mathcal{O}\left(\frac{MN}{2}\log_2 N\right)$. On the whole, this LMMSE equalization method has a complexity of just $\mathcal{O}\left(\frac{MN}{2}\log_2 N + MN\right)$ compared to $\mathcal{O}(M^3N^3)$ of the conventional LMMSE equalization.

3.2 Approximate MAP Detection

From the vectorized representation $\mathbf{y} = \mathbf{H}\mathbf{x} + \mathbf{v}$ in Eq. (10), the MAP decision rule for detection of \mathbf{x} is given by

$$\hat{\mathbf{x}} = \arg \max_{\mathbf{x} \in \mathbb{A}^{MN}} \Pr(\mathbf{x}|\mathbf{y}, \mathbf{H}). \quad (28)$$

When the transmit symbol vectors are equally likely, the decision rule for maximum-likelihood (ML) detection is

$$\hat{\mathbf{x}} = \arg \max_{\mathbf{a} \in \mathbb{A}^{MN}} \Pr(\mathbf{y}|\mathbf{x} = \mathbf{a}, \mathbf{H}) \Pr(\mathbf{x} = \mathbf{a}) = \arg \max_{\mathbf{a} \in \mathbb{A}^{MN}} \frac{1}{|\mathbb{A}|} \Pr(\mathbf{y}|\mathbf{x} = \mathbf{a}, \mathbf{H}). \quad (29)$$

Assuming the noise vector \mathbf{v} to be i.i.d Gaussian, the optimum decision rule is given by

$$\hat{\mathbf{x}} = \arg \min_{\mathbf{x} \in \mathbb{A}^{MN}} \|\mathbf{y} - \mathbf{H}\mathbf{x}\|^2. \quad (30)$$

The complexity of the optimum detector grows exponentially in MN because of the exhaustive enumeration/search involved. Therefore, several suboptimum detection algorithms have been proposed that are efficient with low complexity. In the following, some of the popular low-complexity approximate MAP algorithms for OTFS signal detection are presented.

3.2.1 Message Passing Algorithm

One of the popular detectors reported in the early OTFS literature is an approximate MAP detector based on low-complexity message passing^[11]. The key advantages of this detector are its linear complexity in MN and very good performance. The message passing algorithm involves the computation of approximate a posteriori probability of the modulation symbols by passing messages on a factor graph. The transmitted vector \mathbf{x} is represented by MN variable nodes and the re-

ceived vector \mathbf{y} is represented by MN check nodes in the graph. As noted earlier in Section 2, \mathbf{H} is sparse with only L non-zero elements in any row or column (generally $L \ll MN$ and $L = P$ for non-fractional delays and Dopplers).

Let $\mathcal{I}(r)$ and $\mathcal{J}(c)$ denote the indices corresponding to non-zero elements in the r -th row and c -th column, respectively, such that $|\mathcal{I}(r)| = |\mathcal{J}(c)| = L$ for all rows and columns. In the factor graph, each variable node $x[c]$ has connections with L check nodes $y[r], r \in \mathcal{J}(c)$ and each check node $y[r]$ has connections with L variable nodes $x[c], c \in \mathcal{I}(r)$ as shown in Fig. 5. The symbol-by-symbol decision rule is given by

$$\hat{x}[c] = \arg \max_{a_j \in \mathbb{A}} \frac{1}{|\mathbb{A}|} \Pr(\mathbf{y}|\mathbf{x}[c] = a_j, \mathbf{H}) \approx \arg \max_{a_j \in \mathbb{A}} \prod_{r \in \mathcal{J}(c)} \Pr(y[r]|\mathbf{x}[c] = a_j, \mathbf{H}). \quad (31)$$

This approximation is obtained assuming that the components of vector \mathbf{y} are independent for a given $\mathbf{x}[c]$ because of the sparsity of \mathbf{H} matrix. From the system model, we can write

$$y[r] = x[c]H[r,c] + \underbrace{\sum_{e \in \mathcal{I}(r), e \neq c} x[e]H[r,e]}_{\zeta_{r,c}^{(i)}} + v[r]. \quad (32)$$

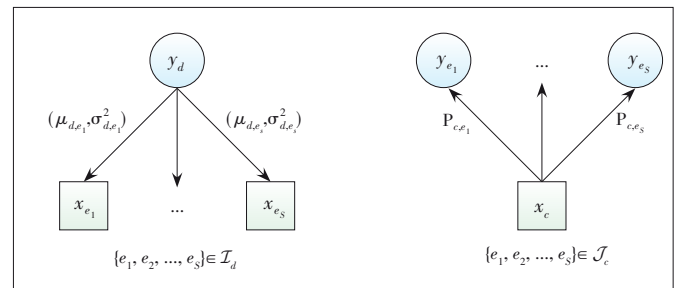
In the i -th iteration, the complete interference plus noise term in Eq. (32) is modelled as a single Gaussian random variable $\zeta_{r,c}^{(i)}$ with mean $\mu_{r,c}^{(i)}$ and variance $(\sigma_{r,c}^{(i)})^2$.

1) Message from check node $y[r]$ to variable node $x[c]$: The check nodes pass mean and variance information to the variable nodes, where

$$\mu_{r,c}^{(i)} = \sum_{e \in \mathcal{I}(r), e \neq c} \sum_{j=1}^{|\mathbb{A}|} p_{e,r}^{(i-1)}(a_j) a_j H[r,e], \quad (33)$$

$$(\sigma_{r,c}^{(i)})^2 = \sum_{e \in \mathcal{I}(r), e \neq c} \left(\sum_{j=1}^{|\mathbb{A}|} p_{e,r}^{(i-1)}(a_j) |a_j|^2 |H[r,e]|^2 - \left| \sum_{j=1}^{|\mathbb{A}|} p_{e,r}^{(i-1)}(a_j) a_j H[r,e] \right|^2 \right) + \sigma^2, \quad (34)$$

and σ^2 is the variance of $v[r]$.



▲ Figure 5. Message passing between variable nodes and check nodes

2) Message from variable node $x[c]$ to check node $y[r]$: The variable nodes compute the probability mass function and pass it to the check nodes. Each component of the probability mass function $p_{(c,r)}^{(i)}$ is given by

$$p_{(c,r)}^{(i)}(a_j) = \Delta \tilde{p}_{(c,r)}^{(i)}(a_j) + (1 - \Delta) \tilde{p}_{(c,r)}^{(i-1)}(a_j), \quad (35)$$

where

$$\tilde{p}_{(c,r)}^{(i)}(a_j) = \prod_{e \in \mathcal{J}(c), e \neq r} \Pr(y[e] | x[c] = a_j, H) = \prod_{e \in \mathcal{J}(c), e \neq r} \frac{\xi_{(i)}(e, c, j)}{\sum_{t=1}^{|A|} \xi_{(i)}(e, c, t)}, \quad (36)$$

$$\xi_{(i)}(e, c, t) = \exp\left(\frac{-|y[e] - \mu_{e,c}^{(i)} - H_{e,c} a_t|^2}{(\sigma_{e,c}^{(i)})^2}\right). \quad (37)$$

3) Compute convergence parameter $\eta^{(i)}$ for some $\gamma > 0$, as

$$\eta^{(i)} = \frac{1}{MN} \sum_{c=1}^{MN} \mathbb{I}\left(\max_{a_j \in \mathbb{A}} p_c^{(i)}(a_j) \geq 1 - \gamma\right), \quad (38)$$

and

$$p_c^{(i)}(a_j) = \prod_{e \in \mathcal{J}(c)} \frac{\xi_{(i)}(e, c, j)}{\sum_{t=1}^{|A|} \xi_{(i)}(e, c, t)}. \quad (39)$$

4) If $\eta^{(i)} < \eta^{(i-1)}$ for $c = 1, 2, \dots, MN$, then update

$$\hat{x}[c] = \arg \max_{a_j \in \mathbb{A}} p_c^{(i)}(a_j). \quad (40)$$

5) Stop the iterations if any one of the following holds:

- The maximum limit set for the number of iterations has reached;

- $\eta^{(i)} = 1$;
- $\eta^{(i)} < \eta^{(s^*)} - \epsilon$ for some small ϵ , where $\eta^{(s^*)} = \max_{s < i} \eta^{(s)}$.

Modified variants of this message passing algorithm have also been proposed. For example, a low complexity variant that exploits channel hardening through match filtering operation on \mathbf{y} and message passing on the resulting system model is presented in Ref. [15]. Another variant in Ref. [17] is presented below.

3.2.2 Gaussian Approximate Message Passing Algorithm

In this variant of message passing, the a posteriori probability of each transmitted symbol is assumed to be Gaussian distributed instead of assuming the inter-symbol interference to be Gaussian as done earlier^[17]. We have

$$\Pr(\mathbf{y} | \mathbf{x}) = \prod_{r=1}^{MN} \Pr(y[r] | \mathbf{x}). \quad (41)$$

As the channel matrix is sparse, we get

$$\Pr(y[r] | \mathbf{x}) = \Pr(y[r] | \mathbf{x}_{\mathcal{I}(r)}), \quad (42)$$

where $\mathbf{x}_{\mathcal{I}(r)}$ contains the elements $x[c]$, $c \in \mathcal{I}(r)$. The Gaussian assumption is that

$$\Pr(y[r] | \mathbf{x}_{\mathcal{I}(r)}) = \frac{1}{\sqrt{2\pi} \sigma} \exp\left(-\frac{1}{2\sigma^2} |y[r] - \mathbf{H}_{\mathcal{I}(r)} \mathbf{x}_{\mathcal{I}(r)}|^2\right), \quad (43)$$

where $\mathbf{H}_{\mathcal{I}(r)}$ is a row vector containing the non-zero elements in r -th row of \mathbf{H} . This approach has been proposed in Ref. [17] and the results presented show that this approach has superior bit error rate (BER) performance with the same complexity order.

3.2.3 Variational Bayes Detection

An iterative algorithm that approximates the optimal MAP detection and has a faster convergence compared to the message passing algorithm has been proposed in Ref. [20]. An approximation of the a posteriori probability $p(\mathbf{x} | \mathbf{y})$ is obtained by using Kullback-Leibler (KL) divergence $\mathcal{D}(q||p)$ and the corresponding evidence lower bound (ELBO) is maximized iteratively using the variational Bayes approach. The convergence is guaranteed because the ELBO maximization problem is convexly resulting in a globally optimum solution. In this way, the marginal distribution for each symbol is obtained which is used for symbol-by-symbol MAP detection. The approximate distribution $q(\mathbf{x})$ is obtained by searching over a family of distributions \mathcal{Q} such that

$$q^*(\mathbf{x}) = \arg \max_{q \in \mathcal{Q}} \mathcal{D}(q||p) = \arg \max_{q \in \mathcal{Q}} \underbrace{E_q[-\ln q(\mathbf{x}) + \ln p(\mathbf{x} | \mathbf{y})]}_{\mathcal{L}}. \quad (44)$$

The ELBO is given by \mathcal{L} which is the expectation over \mathbf{x} having distribution $q(\mathbf{x})$. In particular, when a family \mathcal{Q} with mutually independent variables is considered,

$$q(\mathbf{x}) = \prod_{i=1}^{MN} q_i(x[i]). \quad (45)$$

$q^*(x[i])$ is obtained iteratively $i = 1, 2, \dots, MN$, and the symbols are detected as

$$\hat{x}[i] = \arg \max_{s[i] \in \mathbb{A}} q_i^*(x[i]). \quad (46)$$

In addition to having complexity lower than that of MAP detection, this detection method has performance significantly close to the performance of MAP detection.

3.2.4 Hybrid MAP and PIC Detection

Another approximation to the MAP detection using a partitioning method based on path gains has been proposed in Ref. [16]. The hybrid MAP-PIC algorithm is a combination of both symbol-by-symbol MAP detection and message passing algorithm. The received symbols are partitioned into two subsets based on the path gains of the channel. On one part with good path gains MAP detection is used, and on the remaining part parallel interference cancellation (PIC) method is used. Define the following sets: $\mathbb{H}^{(i)} \triangleq \{h_j | 1 \leq j \leq P, j \neq i\}$, $\mathbb{Y}_{k,l} \triangleq \{y[(k + \beta_j)_N, (l + \alpha_j)_M] | 1 \leq j \leq P\}$, $\mathbb{X}_{k,l}^{(i)} \triangleq \{y[(k + \beta_i - \beta_j)_N, (l + \alpha_i - \alpha_j)_M] | 1 \leq j \leq P, j \neq i\}$, where P is the number of channel paths and i is the path index. The P received symbols that are associated with the transmitted symbol $x[k, l]$ are in set $\mathbb{Y}_{k,l}$. Similarly, the $P - 1$ transmitted symbols, other than $x[k, l]$, corresponding to the received symbol $\mathbb{Y}_{k,l}[i]$ are in set $\mathbb{X}_{k,l}^{(i)}$. The path gains in $\mathbb{H}^{(i)}$ are arranged in decreasing order such that $|h_m|^2 > |h_n|^2$ when $m < n$. The set $\mathbb{X}_{k,l}^{(i)}$ is partitioned into two subsets by enumerating different possible combinations of S (where S is the size of the first subset with good path gains) as follows:

$$\widetilde{\mathbb{X}}_{k,l}^{(i)} \triangleq \{\mathbb{X}_{k,l}^{(i)}[j] | 1 \leq j \leq S\}, \quad (47)$$

$$\bar{\mathbb{X}}_{k,l}^{(i)} \triangleq \{\mathbb{X}_{k,l}^{(i)}[j] | S + 1 \leq j \leq P - 1\}. \quad (48)$$

It is proposed to perform MAP detection on $\widetilde{\mathbb{X}}_{k,l}^{(i)}$ and PIC on $\bar{\mathbb{X}}_{k,l}^{(i)}$. The message passing algorithm that we discussed earlier is a special case of Hybrid-MAP-PIC detection when $S = 0$. Results have shown that choosing $S = P/2$ gives good error performance. A trade-off can be established between BER performance and computation complexity by choosing a suitable value for S .

3.2.5 MCMC Sampling Based Detection

This detection algorithm proposed in Ref. [8] uses the Markov chain Monte Carlo (MCMC) sampling method to obtain an approximate solution to Eq. (28). The joint probability distribution is given by

$$\Pr(\mathbf{x}|\mathbf{y}, \mathbf{H}) = \Pr(x_1, x_2, \dots, x_{MN}|\mathbf{y}, \mathbf{H}) \propto \exp\left(-\frac{\|\mathbf{y} - \mathbf{H}\mathbf{x}\|^2}{\sigma^2}\right). \quad (49)$$

The algorithm starts by initializing a random initial vector $\mathbf{x}^{(t=0)}$, where t denotes the iteration number. The MN coordinates of the \mathbf{x} vector are updated in each iteration based on the coordinates of the previous iteration as follows:

$$\begin{aligned} \mathbf{x}_1^{(t+1)} &\sim \Pr(x_1|x_2^{(t)}, x_3^{(t)}, \dots, x_{MN}^{(t)}, \mathbf{y}, \mathbf{H}), \\ \mathbf{x}_2^{(t+1)} &\sim \Pr(x_2|x_1^{(t)}, x_3^{(t)}, \dots, x_{MN}^{(t)}, \mathbf{y}, \mathbf{H}), \\ \mathbf{x}_3^{(t+1)} &\sim \Pr(x_3|x_1^{(t)}, x_2^{(t)}, x_4^{(t)}, \dots, x_{MN}^{(t)}, \mathbf{y}, \mathbf{H}), \text{ and} \end{aligned}$$

$$\mathbf{x}_{MN}^{(t+1)} \sim \Pr(x_{MN}|x_1^{(t)}, x_2^{(t)}, \dots, x_{MN-1}^{(t)}, \mathbf{y}, \mathbf{H}).$$

After updating over a certain number of iterations, the distribution obtained approximately converges to the distribution in Eq. (49). For a received vector, the symbol vector which has minimum ML cost $\|\mathbf{y} - \mathbf{H}\mathbf{x}\|^2$ in all the iterations is chosen as the detected symbol vector. A modification to this has also been proposed to reduce the number of iterations and also to overcome the phenomenon of stalling seen in the Gibbs sampling method at high SNRs which limits the BER performance. The modified joint distribution involves a temperature parameter α chosen based on the operating SNR and is given by

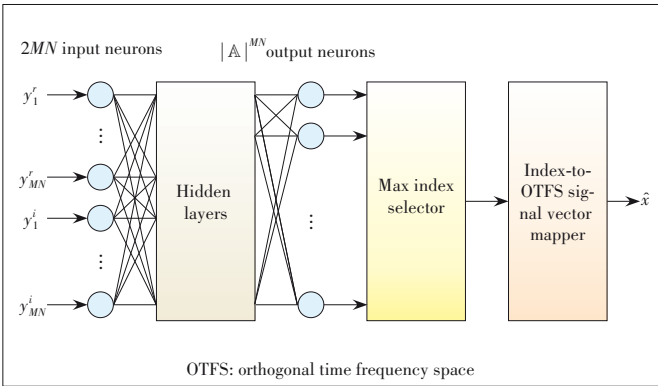
$$\Pr(\mathbf{x}|\mathbf{y}, \mathbf{H}) \propto \exp\left(-\frac{\|\mathbf{y} - \mathbf{H}\mathbf{x}\|^2}{\sigma^2 \alpha^2}\right). \quad (50)$$

Alternately, the sampling can be randomized by updating the parameters in each iteration using the conventional Gibbs sampling method with probability q (e.g., $q = \frac{1}{MN}$) and obtaining samples from a uniform distribution with probability $1 - q$. This randomized sampling has been shown to avoid stalling problems and achieve good BER performance.

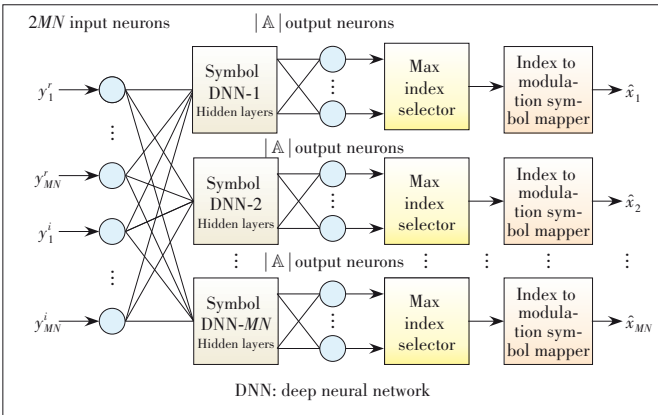
3.3 Neural Networks Based Detection

Apart from the detection methods based on conventional approaches, detectors based on DNN have been proposed recently. Two DNN approaches have been presented in Ref. [18]. One approach is to use a single fully-connected DNN to detect the signal vector. The detection problem is formulated as a multi-class classification problem where each class corresponds to each vector in the transmitted signal set, enabling joint detection of the transmitted symbol vector. The number of input neurons in the network is decided by the size of the received vector (MN) and the number of output neurons is decided by the size of the multi-dimensional modulation alphabet ($|\mathbb{A}|^{MN}$). This approach requires a large number of parameters to be learned and is computationally complex because of the exponential growth in the number of output neurons with the size of transmit symbol vector. The architecture of this fully connected DNN is shown in Fig. 6. The real and imaginary parts of the received vector \mathbf{y} are given as input to the DNN. The activation function used in the output layer is Softmax activation so that the output of each output neuron gives the probability of the corresponding transmitted signal vector and all these probabilities sum to one. The detected symbol vector is the one that has maximum probability.

Another architecture that uses multiple DNNs is shown in Fig. 7. In this approach, each symbol in the transmitted vector is detected by an individual DNN. In this way, each DNN



▲ Figure 6. Full deep neural network (DNN) architecture for detection



▲ Figure 7. Symbol DNN architecture for detection

has the number of output neurons growing linearly in the size of modulation alphabet ($|\mathbb{A}|$). Also, the number of DNNs grows linearly with the size of the transmit symbol vector (MN). This symbol-DNN architecture does symbol-by-symbol detection at lower complexity and achieves BER performance almost the same as that of full-DNN. Each DNN uses Softmax activation in the output layer and obtains probabilities corresponding to each symbol in \mathbb{A} .

The training of the DNNs is done by pseudo-randomly generating a set of training examples \mathbf{x}_T which are known both at the transmitter and the receiver. These training examples are sent to the receiver through the channel. The transmitted signal vector \mathbf{x}_T and the corresponding received signal vector \mathbf{y} form the training pair at the receiver. The real and imaginary parts of \mathbf{y} are given as input to the DNNs. The DNN trained in this manner learns the mapping from the received vector to the corresponding symbol in the transmitted vector. Another approach of using neural networks for signal detection has been reported in Ref. [19], where the two-dimensional structure of the OTFS frame with data augmentation based pre-processing is given as input to two-dimensional convolutional neural networks (CNN) for signal detection.

The benefits of using DNNs for signal detection can be predominantly seen when there are deviations in the noise model from the standard i.i.d. Gaussian model. In situations

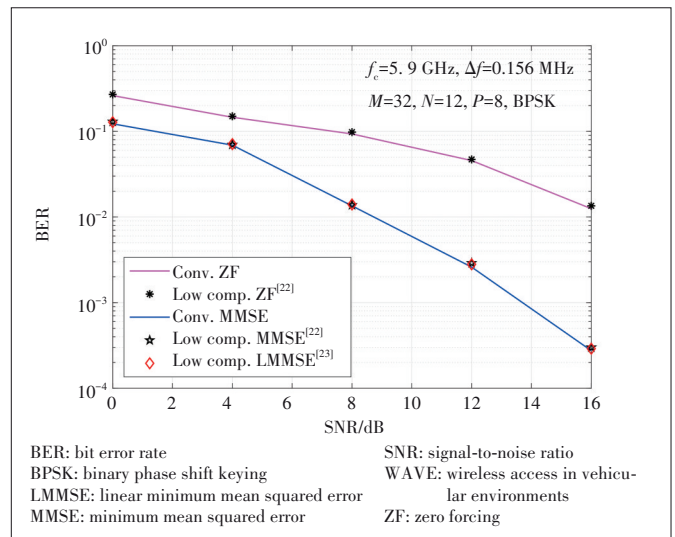
where there are deviations from the Gaussian as well as independence assumptions in the standard noise model, DNN based detection could outperform conventional ML detection. This is because ML detection is optimum only for the standard i.i.d. Gaussian noise model and the DNNs have the ability to learn the underlying deviations in the model.

3.4 Performance Results

In this subsection, we present the BER performance of some of the detectors presented in the previous subsections, assuming perfect DD channel knowledge at the receiver. The system parameters considered are according to the IEEE.802.11p standard for wireless access in vehicular environments (WAVE)^[52]. A carrier frequency of 5.9 GHz with a subcarrier spacing of 0.156 MHz, a maximum speed of 220 km/h, and a multipath channel with $P = 5$ paths are considered. BPSK modulation alphabet is used with a frame size of $M = 32$ and $N = 12$.

Fig. 8 shows the BER performance of the linear detectors including conventional MMSE/ZF detectors and low-complexity MMSE/ZF detectors. It can be observed from Fig. 8 that the performance of the conventional MMSE detector and the low-complexity MMSE detectors in Refs. [22] and [23] are the same. However, the detectors in Refs. [22] and [23] achieve this with significantly lower complexities compared to the conventional MMSE detector complexity. This is illustrated in Fig. 9 where the computational complexities (in the number of real operations) for these detectors are plotted.

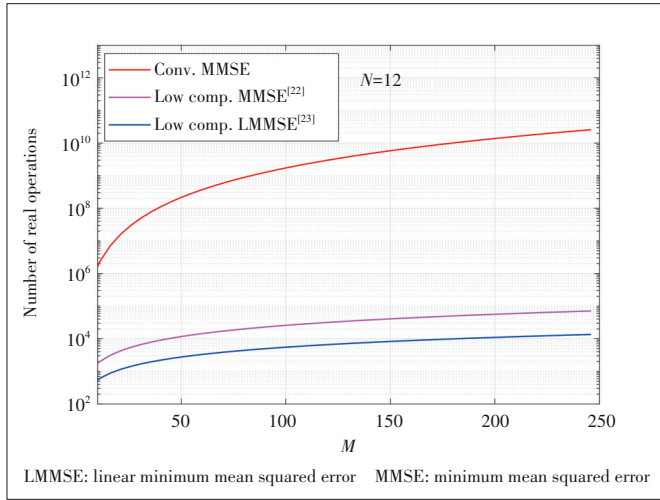
The BER performance of the message passing detector in Ref. [11] and the symbol-DNN based detector in Ref. [18] are shown in Fig. 10. MMSE detection performance is also shown for comparison. In this figure, a system with a carrier frequency of 4 GHz, subcarrier spacing of 15 kHz, OTFS frame size of $M = N = 16$, and a uniform power delay profile



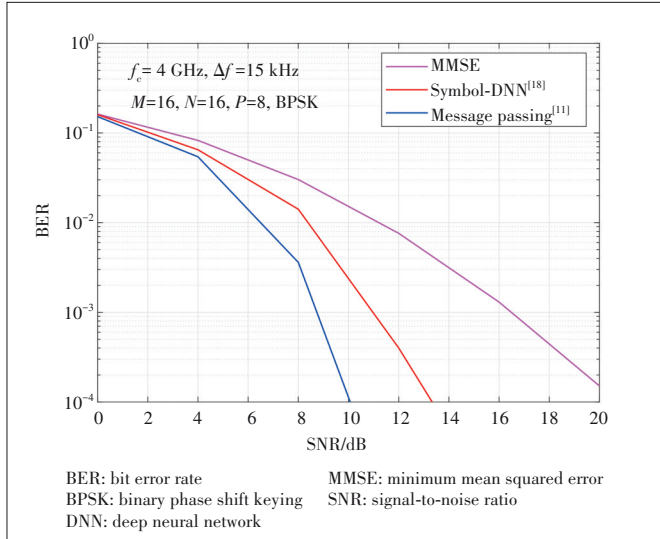
▲ Figure 8. BER performance of linear OTFS detectors for IEEE 802.11p WAVE channel model

channel with $P = 8$ are considered. The delay-Doppler profile considered is shown in Table 1. For the message passing algorithm, a damping factor of $\Delta = 0.6$ and maximum iterations of 30 are used. For the symbol-DNN based detection, the parameters of the neural network are shown in Table 2. It can be seen from Fig. 10 that the symbol-DNN performs better than the MMSE detector, and the message passing detector gives the best performance among them.

Next, the performance superiority of DNN-based detection compared to ML detection in correlated noise is illustrated in Fig. 11. This figure shows the BER performance of the ML



▲ Figure 9. Computational complexity of conventional MMSE and low-complexity MMSE detectors



▲ Figure 10. BER performance of MMSE, message passing, and symbol-DNN based detectors

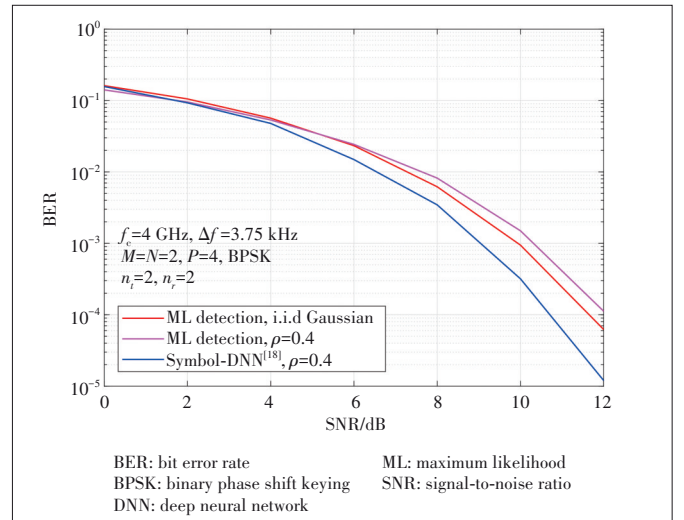
▼ Table 1. Delay-Doppler profile considered in Figure 10

Path (i)	1	2	3	4	5	6	7	8
τ_i (μ s)	0	4.16	8.32	12.48	16.64	20.8	24.96	29.12
ν_i (ms)	0	0	938.5	938.5	938.5	1 875	1 875	1 875

▼ Table 2. Parameters of symbol-DNN detector in Figure 10

Parameters	Symbol-DNN
Number of input neurons	$2MN = 512$
Number of output neurons	$ A = 2$
Number of hidden layers	1
Number of neurons in hidden layers	256
Hidden layer activation	ReLU
Output layer activation	Softmax
Optimization	Adam
Loss function	Binary cross entropy
Training SNR	10 dB
Number of training examples	50 000
Number of epochs	50

DNN: deep neural network ReLU: Rectified Linear Unit SNR: signal-to-noise ratio



▲ Figure 11. BER performance of ML detection and symbol-DNN based detection in 2x2 MIMO-OTFS with correlated noise

detector and symbol-DNN detector for a MIMO-OTFS system when the noise is correlated. The correlated noise vector is taken to be $\mathbf{v}_c = \mathbf{N}_c \mathbf{v}$, where \mathbf{v} is the i.i.d Gaussian noise vector and \mathbf{N}_c is the correlation matrix $\mathbf{N}_c =$

$$\begin{bmatrix} 1 & \rho & \rho^2 & \cdots & \rho^{n_r-1} \\ \rho & 1 & \rho & \cdots & \rho^{n_r-2} \\ \vdots & \vdots & \vdots & \ddots & \vdots \\ \rho^{n_r-1} & \rho^{n_r-2} & \cdots & \cdots & 1 \end{bmatrix}, \text{ given by Ref. [53], where } \rho$$

is the correlation coefficient ($0 \leq \rho \leq 1$), n_t is the number of transmit antennas, and n_r is the number of receive antennas. The following system parameters are considered in Fig. 11: carrier frequency of 4 GHz, subcarrier spacing of 3.75 kHz, frame size of $M = N = 2$, uniform power delay profile channel with $P = 4$, MIMO configuration with $n_t = n_r = 2$, and a correlation coefficient $\rho = 0.4$. The symbol-DNN architecture has an input layer with 16 nodes, one hidden layer with 32 nodes, and an output layer with 2 nodes. The hidden layer has ReLU activation and the output layer has Softmax activa-

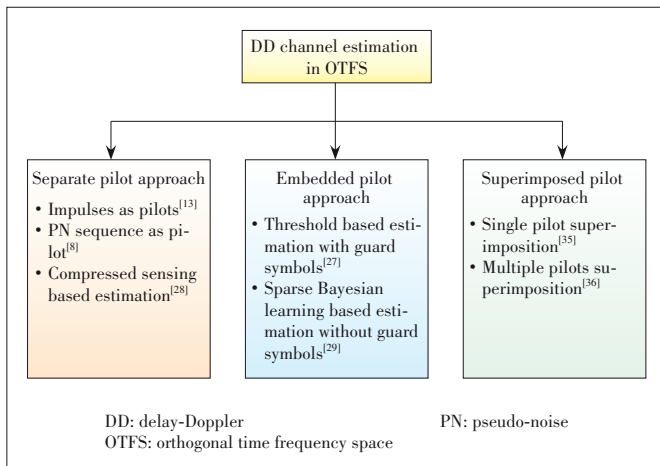
tion. The DNN is trained at an SNR of 8 dB for 60 epochs with 50 000 training examples. It can be seen from Fig. 11 that the symbol-DNN based detector outperforms the ML detector by almost 1 dB at BER of 10^{-4} . This is because the ML detector is optimal only when the noise is i.i.d Gaussian and is suboptimal in correlated noise. On the other hand, the symbol-DNN based detector performs well as it effectively learns the noise correlation leading to superior BER performance.

4 DD Channel Estimation

The task of channel estimation at the receiver is crucial as signal detection operation requires the knowledge of the channel state information. In OTFS, signal detection is carried out in the DD domain. In the system model in Eq. (10), knowledge of the DD channel matrix \mathbf{H} is needed for detection. In order to estimate \mathbf{H} , \mathbf{x} vector consisting of known pilot symbols is sent. Given the knowledge of the pilot symbol(s) in \mathbf{x} and the observation vector \mathbf{y} , channel estimation algorithms estimate \mathbf{H} . For the purpose of exposition, we classify the channel estimation approaches into three broad categories based on the OTFS frame pattern used to transmit the pilot and data symbols. Fig. 12 shows this classification consisting of 1) separate pilot approach, 2) embedded pilot approach, and 3) superimposed pilot approach. In the first approach, pilot frames consisting of only pilot symbols are used for channel estimation. The estimated channel matrix obtained during the pilot frame is used for detection during data frames. The second approach involves embedding both pilot and data symbols in a frame. In the third approach, pilot symbols are superimposed on data symbols. Some of the channel estimation techniques/algorithms employing these approaches are presented in the following subsections.

4.1 Separate Pilot Approach

As mentioned earlier, in this approach, separate frames



▲ Figure 12. DD channel estimation approaches in OTFS

are used for sending pilot symbols and data symbols. A pilot frame consists of only pilot symbol(s). One pilot frame per spatial coherence interval of the DD channel is sent. The channel estimated during the pilot frame is used for the detection of symbols in the data frames in that coherence interval. In the following, we present three-channel estimation methods using this approach.

4.1.1 Impulse Based Channel Estimation

In this method, impulses in the DD domain are sent as pilots^[13], i.e., the pilot symbol is given by

$$x_p[k, l] = \begin{cases} 1, & \text{if } (k, l) = (k_p, l_p) \\ 0, & \forall (k, l) \neq (k_p, l_p). \end{cases} \quad (51)$$

For this transmitted pilot, the received signal at the receiver is

$$y_p[k, l] = \frac{1}{MN} \sum_{l'=0}^{M-1} \sum_{k'=0}^{N-1} x_p[k', l'] h_w \left(\frac{k-k'}{NT}, \frac{l-l'}{M\Delta f} \right) + v[k, l] \quad (52)$$

As the receiver knows the pilot locations k_p and l_p a priori, $h_w \left(\frac{k}{NT}, \frac{l}{M\Delta f} \right)$ can be estimated using Eq. (52) and the estimated channel matrix $\hat{\mathbf{H}}$ can be obtained.

4.1.2 PN Pilot Based Estimation

Instead of impulses as pilots, this method uses PN sequence as a pilot^[8]. The estimation is done in the discrete domain and the parameters to be estimated are delay tap τ_i , Doppler shift ν_i , and channel fade coefficient h'_i . The input-output relation for a P path channel in the time domain can be obtained as

$$y(t) = \sum_{i=1}^P h_i x(t - \tau_i) e^{j2\pi\nu_i(t - \tau_i)} + v(t) = \sum_{i=1}^P h'_i e^{j2\pi\nu_i t} x(t - \tau_i) + v(t), \quad (53)$$

where $h'_i = e^{-j2\pi\nu_i\tau_i}$.

Let \mathcal{H} denote the vector space of complex-valued functions on the set of finite integers $\mathbb{Z}_{N_p} = \{0, 1, \dots, N_p - 1\}$ with an inner product defined as

$$\langle g_1, g_2 \rangle = \sum_{n \in \mathbb{Z}_{N_p}} g_1[n] g_2^*[n], \quad g_1, g_2 \in \mathcal{H}. \quad (54)$$

A signal is transmitted which is given by

$$S_A(t) = \sum_{n=0}^{M-1} S[n \bmod N_p] \text{sinc}(Wt - n), \quad (55)$$

where $S \in \mathcal{H}$, $M = N_p + \lceil W \max(\tau_i) \rceil \geq N_p$. For some $S \in \mathcal{H}$ that is transmitted, the received sequence $R[n]$ is

$$R[n] = \sum_{i=1}^P \alpha_i e(\omega_i n) S[n - \delta_i] + v[n], n \in \mathbb{Z}_{N_p}, \quad (56)$$

where $e(t) = e^{j \frac{2\pi}{N_p} t}$, $\delta_i, \omega_i \in \mathbb{Z}_{N_p}$, $\alpha_i \in \mathbb{C}$, and $v[n] \in \mathcal{H}$. Eq. (56) can be simplified as

$$R[n] = e(\omega_0 n) S[n - \delta_0] + v[n], \quad (57)$$

such that $(\delta_0, \omega_0) \in \mathbb{Z}_{N_p} \times \mathbb{Z}_{N_p}$. The (δ_0, ω_0) pairs are estimated using the time-frequency shift problem. A matched filter matrix for R and S is defined as

$$\mathcal{M}(R, S)[\delta, \omega] = \langle R[n], e(\omega n) S[n - \delta] \rangle = \begin{cases} 1 + \epsilon'_{N_p}, & \text{if } (\delta, \omega) = (\delta_0, \omega_0) \\ \epsilon_{N_p}, & \text{if } (\delta, \omega) \neq (\delta_0, \omega_0), \end{cases} \quad (58)$$

where $|\epsilon'_{N_p}| \leq \frac{1}{\sqrt{N_p}}$ and $|\epsilon_{N_p}| \leq \frac{C+1}{\sqrt{N_p}}$ for some positive constant C . Thus, compute $\mathcal{M}(R, S)$ and choose (δ_0, ω_0) such that $\mathcal{M}(R, S)[\delta_0, \omega_0] \approx 1$. Once δ_0 and ω_0 are estimated, h'_i , τ_i and ν_i can be obtained.

4.1.3 Compressed Sensing Based Estimation

The channel estimation problem can be formulated as a sparse signal recovery problem using compressed sensing based methods like orthogonal matching pursuit (OMP) and modified sub-space pursuit (MSP)^[28]. The channel is estimated by sending a pilot matrix X_p in the DD domain with i.i.d Gaussian random sequences as pilots. The system model is rewritten as

$$\mathbf{y}_p = X_p \mathbf{h} + \mathbf{v}, \quad (59)$$

such that $X_p \in \mathbb{C}^{MN \times MN}$ and $\mathbf{h} \in \mathbb{C}^{MN \times 1}$ have P non-zero elements. The channel estimation problem as a sparse signal recovery problem is given by

$$\min \|\mathbf{h}\|_0 \quad \text{s.t.} \quad \mathbf{y}_p = X_p \mathbf{h} + \mathbf{v}. \quad (60)$$

OMP algorithm is used when the knowledge of the number of paths P is available. Initialize $\mathbf{h}^0 = \mathbf{0}$, $S^0 = \emptyset$, and $\mathbf{r}^0 = \mathbf{y}_p$. The following operations are performed in the i th iteration. The indices of the highest correlated columns are obtained as $T^i = \arg \max_j |\mathbf{X}_p^H \mathbf{r}^{i-1}|$, and the support is updated as $S^i = S^{i-1} \cup T^i$. The non-zero values corresponding to the support are $\mathbf{h}_{S^i} = (\mathbf{X}_p^{S^i})^\dagger \mathbf{y}_p$, where $(\cdot)^\dagger$ is the pseudo-inverse operator.

Finally, the residue is updated as $\mathbf{r}^i = \mathbf{y}_p - \mathbf{X}_p^{S^i} \mathbf{h}_{S^i}$. Stop the iterations when $\|\mathbf{r}^i\|_2$ is less than a threshold ϵ and obtain

the estimate as $\hat{\mathbf{h}}_{S^i} = (\mathbf{X}_p^{S^i})^\dagger \mathbf{y}_p$ and $\hat{\mathbf{h}}_{\bar{S}^i} = \mathbf{0}$.

When the knowledge of the number of channel paths P is not known, the subspace pursuit algorithm is modified to estimate the channel and the corresponding support using Algorithm 1. \mathbf{y}_p, X_p and ϵ are given as input and $\hat{\mathbf{h}}$ is obtained as output.

Algorithm 1. MSP based channel estimation^[28]

Inputs: \mathbf{y}, X, ϵ

Initialize: $i = 1, \mathbf{r}_1 = \mathbf{y}$

while $(\|\mathbf{r}_i\|_2 - \|\mathbf{r}_{i-1}\|_2 > \epsilon)$ **do**

Initialize: $t = 0, \mathbf{h}_i^0 = \mathbf{0}, S_i^0 = \{l_1^0, \dots, l_i^0\}$ are indices of i max. entries of $|\mathbf{X}^H \mathbf{y}|$, $\mathbf{b}_i^0 = \mathbf{X}_{S_i^0}^\dagger \mathbf{y}$, $\mathbf{r}_i^0 = \mathbf{y} - \mathbf{X}_{S_i^0} \mathbf{b}_i^0$

while $t \leq t_{\max}$ **do**

$t = t + 1$

$\tilde{S}_i^t = S_i^t \cup \Theta_i^t$, where Θ_i^t is a set of i indices corresponding to the i max. entries of $|\mathbf{X}^H \mathbf{r}_i^{t-1}|$

$\mathbf{u}_i^t = \mathbf{X}_{\tilde{S}_i^t}^\dagger \mathbf{y}$

$S_i^t = \{l_1^t, \dots, l_i^t\}$ are i entries from \tilde{S}_i^t which leads to i max. entries of $|\mathbf{u}_i^t|$

$\mathbf{b}_i^t = \mathbf{X}_{S_i^t}^\dagger \mathbf{y}$

$\mathbf{r}_i^t = \mathbf{y} - \mathbf{X}_{S_i^t} \mathbf{b}_i^t$

$\mathbf{r}_i = \mathbf{r}_i^{t_{\max}}$

$S_i = S_i^{t_{\max}}$

$i = i + 1$

Output: Estimated channel is $\hat{\mathbf{h}}_{S_i} = \mathbf{X}_{S_i}^\dagger \mathbf{y}$ and $\hat{\mathbf{h}}_{\bar{S}_i} = \mathbf{0}$

4.2 Embedded Pilot Approach

In this approach, instead of allocating an entire OTFS frame for pilot transmission, pilot symbols are transmitted in the same frame as data symbols with guard symbols around to prevent interference between pilot and data symbols. If no guard symbols are provided, then more sophisticated algorithms may be needed to handle the interference. In the following, we present two estimation algorithms for the embedded pilot approach. The first algorithm is applicable when guard symbols are provided. The second algorithm, based on sparse Bayesian learning, is applicable for embedded frames without guard symbols.

4.2.1 Embedded Pilot Based Estimation

In the embedded pilot based estimation^[27], let (k_p, l_p) be the pilot location such that $0 \leq k_p \leq N - 1$ and $0 \leq l_p \leq M - 1$. Define $\alpha = \max\{\alpha_i\}$ corresponding to the largest delay and $\beta = \max\{\beta_i\}$ corresponding to the largest Doppler. More

precisely, it is better to choose (k_p, l_p) such that $0 \leq l_p - \alpha \leq l_p \leq l_p + \alpha \leq M - 1$, and $0 \leq k_p - 2\beta \leq k_p \leq k_p + 2\beta \leq N - 1$.

The pilot, guard, and data symbols in an OTFS frame are arranged as follows (see Fig. 13 for an example):

$$x[k, l] = \begin{cases} x_p & k = k_p, l = l_p \\ 0 & k_p - 2\beta \leq k \leq k_p + 2\beta, l_p - \alpha \leq l \leq l_p + \alpha. \\ x_d[k, l] & \text{otherwise.} \end{cases} \quad (61)$$

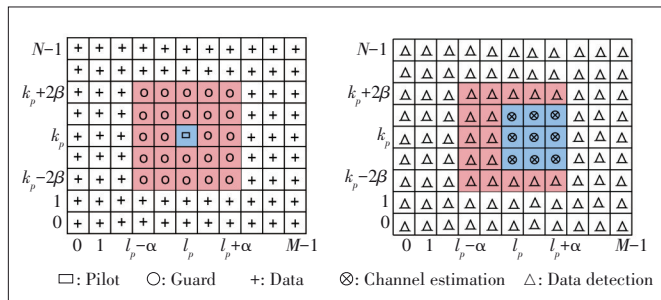
At the receiver, the subgrid in $y[k, l]$ used for channel estimation is given by $[k_p - \beta \leq k \leq k_p + \beta, l_p \leq l \leq l_p + \alpha]$. Within this subgrid, if $|y[k, l]| \geq \mathcal{T}$ for a detection threshold $\mathcal{T} > 0$, then $\hat{h}[k - k_p, l - l_p] = y[k, l]/x_p$ and $\hat{h}[k - k_p, l - l_p] = 0$ otherwise. If a path exists, then it must be seen in the received frame as a scaled version of the pilot plus Gaussian noise. It has been shown that choosing $\mathcal{T} = 3\sigma$ gives good estimation where σ^2 is the noise variance. An extension to this method has also been proposed in Ref. [27] considering the fractional Doppler scenario. A method to select a threshold value based on the receiver operating characteristics (ROC) curve has been demonstrated in Ref. [32].

4.2.2 Sparse Bayesian Learning Based Estimation

In this method, the problem of channel estimation is converted to a problem of sparse signal recovery by exploiting the sparsity of the channel in the DD domain^[29]. This method does not require guard symbols and uses pilot SNR to be the same as data SNR. This approach considers the case of fractional Dopplers as well. The structure of the OTFS frame is given by (see Fig. 14 for an example)

$$x[k, l] = \begin{cases} x_p, k_p - 2\beta - Q \leq k \leq k_p + 2\beta + Q, l_p - \alpha \leq l \leq l_p + \alpha \\ x_d[k, l], \text{ otherwise} \end{cases}, \quad (62)$$

where k_p and l_p are chosen to be $N/2$ and $M/2$, respectively, and Q is a parameter that approximates the effect of Doppler. Results in Ref. [27] show that the channel approximation is



▲ Figure 13. Transmit and receive symbol pattern for embedded pilot based channel estimation^[27]

good when $Q = 5$. Further, l_r is a parameter that obtains a trade-off between the error performance and pilot overhead. At the receiver, $y[k, l]$, $k \in [k_p - \beta, k_p + \beta]$, $l \in [l_p, l_p + l_r]$ are used for channel estimation. The system model for $L = (2\beta + 2Q + 1) \times (\alpha + 1)$ pilot symbols $(x_p[k, l])$ is modified as

$$\mathbf{y} = (\mathbf{X} \odot \mathbf{B}) \mathbf{h} + \mathbf{v} = \mathbf{\Phi} \mathbf{h} + \mathbf{v}, \quad (63)$$

where $\mathbf{X} \in \mathcal{C}^{MN \times L}$, $\mathbf{h} \in \mathcal{C}^{L \times 1}$, and $\mathbf{v} \in \mathcal{C}^{MN \times 1}$. \mathbf{B} is the phase compensation matrix which is a block diagonal matrix with the conjugate of the phase terms on the diagonal, and \odot is Hadamard product operator. The noise in Eq. (63) is assumed to be Gaussian with zero mean and variance $1/\nu_0$, $\Pr(\mathbf{v}|\nu_0) = \mathcal{N}(\mathbf{v}|\mathbf{0}, \nu_0^{-1} \mathbf{I})$. The precision parameter ν_0 is assumed to be Gamma distributed with parameters a and b . With this assumption, the distribution of the received vector is given as $\Pr(\mathbf{y}|\mathbf{\Phi} \mathbf{h}, \nu_0^{-1} \mathbf{I})$. By modelling the conjugate prior as per the Bayesian estimation framework, we get

$$\Pr(\mathbf{h}|\nu) = \mathcal{N}(\mathbf{0}, \mathbf{\Lambda}), \quad (64)$$

$$\Pr(\nu; \lambda) = \prod_{i=1}^L \Gamma(\nu_i | 1, \frac{\lambda}{2}), \quad (65)$$

where $\mathbf{\Lambda} = \text{diag}(\nu)$ is the covariance matrix and ν_i is the variance of h_i . All the h_i 's are identical with a Laplace sparse prior distribution

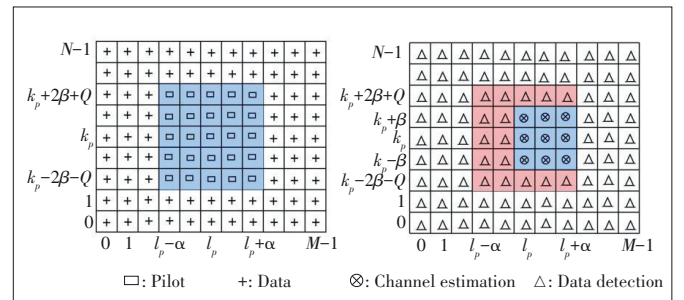
$$\Pr(h_i | \lambda) = \text{Laplace}\left(0, \frac{1}{\sqrt{\lambda}}\right), \quad i = 1, 2, \dots, L. \quad (66)$$

The joint probability distribution of this model is written as

$$\Pr(\mathbf{y}, \mathbf{h}, \nu, \nu_0) = \Pr(\mathbf{y}|\nu) \Pr(\mathbf{h}|\nu) \Pr(\nu) \Pr(\nu_0), \quad (67)$$

and

$$\Pr(\mathbf{h}|\mathbf{y}, \nu, \nu_0) = \mathcal{N}(\mathbf{h}|\boldsymbol{\mu}, \boldsymbol{\Sigma}), \quad (68)$$



▲ Figure 14. Transmit and receive symbol pattern for sparse Bayesian learning based channel estimation^[29]

where $\boldsymbol{\mu} = \mathbf{v}_0 \boldsymbol{\Sigma} \boldsymbol{\Phi}^T \mathbf{y}$ and $\boldsymbol{\Sigma} = (\mathbf{v}_0 \boldsymbol{\Phi}^T \boldsymbol{\Phi} + \boldsymbol{\Lambda}^{-1})^{-1}$. The values of \mathbf{v} and \mathbf{v}_0 are obtained by solving expectation maximization (EM) algorithm as

$$(\hat{\mathbf{v}}, \hat{\mathbf{v}}_0) = \arg \max_{\mathbf{v}, \mathbf{v}_0} E \{ \ln \Pr(\mathbf{y}, \mathbf{h}, \mathbf{v}, \mathbf{v}_0) \}, \quad (69)$$

which gives

$$\hat{v}_i = \frac{\sqrt{1 + 4\lambda(\sum_{ii} + \mu_i^2)} - 1}{2\lambda}, \quad i = 1, 2, \dots, L, \quad (70)$$

$$\hat{\mathbf{v}}_0 = \frac{2a - 2 + MN}{2b + \mathbf{v}_0^{-1} \sum_{i=1}^L (1 - v_i^{-1} \sum_{ii}) + \|\mathbf{y} - \boldsymbol{\Phi} \boldsymbol{\mu}\|_2^2}. \quad (71)$$

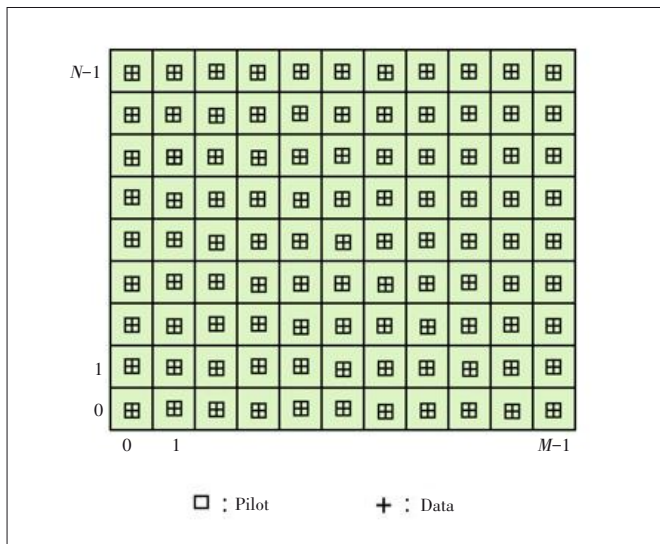
After obtaining $\boldsymbol{\mu}$, the first $P(2Q + 1)$ largest values in $\boldsymbol{\mu}$ are selected as \mathbf{h} .

4.3 Superimposed Pilot Approach

In this approach, pilot symbols are superimposed on data symbols in an OTFS frame. For example, each bin in the DD grid has a data symbol and a pilot symbol superimposed on it as shown in Fig. 15^[35]. Fig. 16 shows another example where all bins have data symbols and only one among them has a superimposed pilot symbol^[36].

4.3.1 Superimposed Pilots Based Estimation in Ref. [35]

In this method of estimation, low-powered pilot symbols are superimposed on the data symbols in the DD grid (Fig. 15). The mutual interference between the pilot and the data symbols is handled by optimum selection of pilot SNR and by adopting an iterative approach that iterates between channel



▲ Figure 15. Transmit symbol pattern in superimposed pilot scheme in Ref. [35]

estimation and data detection. The system model considered is

$$\mathbf{y} = \mathbf{X} \mathbf{h} + \mathbf{v}, \quad (72)$$

where $\mathbf{X} \in \mathcal{C}^{MN \times P}$, $\mathbf{h} \in \mathcal{C}^{P \times 1}$, and $\mathbf{v} \in \mathcal{C}^{MN \times 1}$. When the pilot symbols are superimposed on the data symbols, the system model is given by

$$\mathbf{y} = \mathbf{X}_p \mathbf{h} + \underbrace{\mathbf{X}_d \mathbf{h} + \mathbf{v}}_{\mathbf{v}_d} = \mathbf{X}_p \mathbf{h} + \mathbf{v}_d, \quad (73)$$

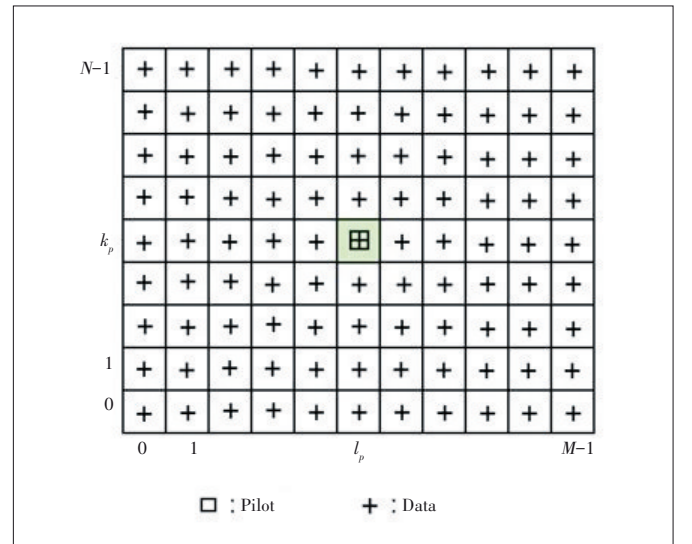
where \mathbf{X}_p corresponds to pilot symbols, \mathbf{X}_d corresponds to data symbols, and \mathbf{v}_d is the noise plus interference term having mean $\boldsymbol{\mu}_{\mathbf{v}_d} = \mathbf{0}_{MN \times 1}$ and covariance

$$\mathbf{C}_{\mathbf{v}_d} = \left(\left(\sum_{i=1}^P \sigma_{h_i}^2 \right) \sigma_d^2 + \sigma_v^2 \right) \mathbf{I}_{MN}, \quad (74)$$

where $\sigma_d^2 = E \left[|x_d(k, l)|^2 \right]$, $\sigma_{h_i}^2$ is the variance of i th channel coefficient, and σ_v^2 is the noise variance. Under these assumptions, the MMSE estimate of the channel using superimposed pilots is given by

$$\hat{\mathbf{h}}_{sp} = \left(\mathbf{X}_p^H \mathbf{C}_{\mathbf{v}_d}^{-1} \mathbf{X}_p + \mathbf{C}_h^{-1} \right)^{-1} \mathbf{X}_p^H \mathbf{C}_{\mathbf{v}_d}^{-1} \mathbf{y}, \quad (75)$$

where $\mathbf{C}_h = \text{diag}(\sigma_{h_1}^2, \sigma_{h_2}^2, \dots, \sigma_{h_p}^2)$. Message passing algorithms along with the MMSE estimated channel are used to detect the data symbols $\hat{\mathbf{X}}_d^{(0)}$. This is used as initialization of \mathbf{X}_d for an iterative channel estimation algorithm which is more robust to the interference than the MMSE estimate. With this, the system model in Eq. (73) can be rewritten as



▲ Figure 16. Transmit symbol pattern in superimposed pilot scheme in Ref. [36]

$$\mathbf{y} = (\mathbf{X}_p + \hat{\mathbf{X}}_d^{(0)})\mathbf{h} + (\mathbf{X}_d - \hat{\mathbf{X}}_d^{(0)})\mathbf{h} + \mathbf{v} = \mathbf{X}_{x_p, \hat{x}_d}^{(0)}\mathbf{h} + \boldsymbol{\xi}_w^{(0)}. \quad (76)$$

Here, the data-aided pilot is given by $\mathbf{X}_{x_p, \hat{x}_d}^{(0)}$ and the interference plus noise term is given by $\boldsymbol{\xi}_w^{(0)}$, where

$$\mathbf{X}_{x_p, \hat{x}_d}^{(0)} = \mathbf{X}_p + \hat{\mathbf{X}}_d^{(0)}, \quad \boldsymbol{\xi}_w^{(0)} = (\mathbf{X}_d - \hat{\mathbf{X}}_d^{(0)})\mathbf{h} + \mathbf{v}. \quad (77)$$

For the system model in Eq. (76), the MMSE channel estimate in the n -th iteration $\hat{\mathbf{h}}^{(n)}$ is obtained using Eq. (75) as

$$\hat{\mathbf{h}}^{(n)} = \left((\mathbf{X}_{x_p, \hat{x}_d}^{(n-1)})^H (\mathbf{C}_{\boldsymbol{\xi}_w}^{(n)})^{-1} \mathbf{X}_{x_p, \hat{x}_d}^{(n-1)} + \mathbf{C}_h^{-1} \right)^{-1} \cdot (\mathbf{X}_{x_p, \hat{x}_d}^{(n-1)})^H (\mathbf{C}_{\boldsymbol{\xi}_w}^{(n)})^{-1} \mathbf{y}, \quad (78)$$

where $\mathbf{C}_{\boldsymbol{\xi}_w}^{(n)} = E[\boldsymbol{\xi}_w^{(n)} \boldsymbol{\xi}_w^{(n)H}]$ is given by

$$\mathbf{C}_{\boldsymbol{\xi}_w}^{(n)} = 2 \left(\sum_{i=1}^P \sigma_{h_i}^2 \right) \sigma_d^2 \mathbf{I}_{MN} + \sigma_v^2 \mathbf{I}_{MN}. \quad (79)$$

Thus, the expression in Eq. (78) gives the channel estimation after n iterations.

4.3.2 Superimposed Pilot Based Estimation in Ref. [36]

A data-aided channel estimation that uses the whole OTFS frame for data transmission scheme with one pilot symbol superimposed on a data symbol in the (k_p, l_p) location of the grid is reported in Ref. [36]. The allocation of symbols in the DD grid is given by

$$x[k, l] = \begin{cases} x_p + x_d[k, l], & k = k_p, l = l_p \\ x_d[k, l], & \text{otherwise} \end{cases}. \quad (80)$$

The energy of the pilot symbol is denoted by $E_p = |x_p|^2$ and the average energy of the data symbol is denoted by $E_d = E[|x[k, l]|^2]$. With this frame structure, the received signal in the DD domain is given by

$$y[k, l] = x_p h_w \left[(k - k_p)_N, (l - l_p)_M \right] + \mathcal{I}_{k,l} + v[k, l], \quad (81)$$

where $\mathcal{I}_{k,l}$ is the interference due to data symbols, given by

$$\mathcal{I}_{k,l} = \sum_{k'=k-\beta}^{k+\beta} \sum_{l'=l-\alpha}^l x[k', l'] h_w \left[(k - k')_N, (l - l')_M \right]. \quad (82)$$

The channel is initially estimated using a modified threshold which incorporates the effect due to $\mathcal{I}_{k,l}$. Using this estimated channel, the data symbols are detected by a sum-product algorithm. The interference term can be simplified as

$$\mathcal{I}_{k,l} = \sum_{i \in \mathcal{Q}_{k,l}} h_i x \left[(k - \beta_i)_N, (l - \alpha_i)_M \right] e^{-j2\pi \frac{\alpha_i \beta_i}{MN}}, \quad (83)$$

where $\mathcal{Q}_{k,l}$ is the set of indices of the data symbols that contribute to $y[k, l]$ such that $|\mathcal{Q}_{k,l}| = P$. From this, the energy of the interference part is obtained as

$$E\{|\mathcal{I}_{k,l}|^2\} = \sum_{i \in \mathcal{Q}_{k,l}} E\{|h_i|^2\} E_s. \quad (84)$$

When $\sum_{i=1}^P E\{|h_i|^2\} = 1$, we get $E\{|\mathcal{I}_{k,l}|^2\} = E_s$. Using the interference energy, the threshold is obtained as

$$\gamma = 3 \left(\sqrt{N_0 + E_s} \right). \quad (85)$$

If $|y[k, l]| \geq \gamma$, the estimates of the channel coefficients can be obtained as

$$\hat{h}_w \left[(k - k_p)_N, (l - l_p)_M \right] = \frac{y[k, l]}{x_p}. \quad (86)$$

The data symbols are detected using the estimated \hat{h}_w by the decision rule:

$$\hat{x}[k, l] = \arg \min_{x[k, l] \in \mathcal{A}} \Pr(x[k, l] | \mathbf{y}). \quad (87)$$

The marginal PDF is obtained by using a sum-product algorithm. After detecting the data symbols, the interference caused by them is cancelled and the resultant symbols are given by

$$\tilde{y}[k, l] = y[k, l] - \sum_{k'} \sum_{l'} \hat{x}[k', l'] \hat{h}_w \left[(k - k')_N, (l - l')_M \right]. \quad (88)$$

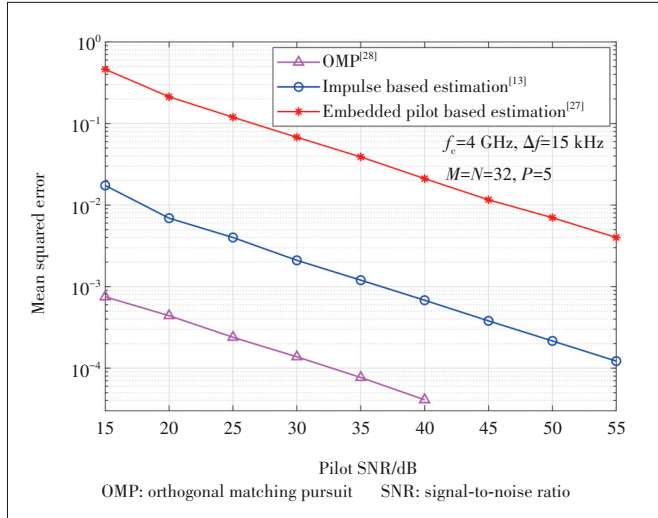
These symbols would contain only the pilot information if the interference was completely cancelled. However, due to imperfect estimates, this method of channel estimation followed by data detection and interference cancellation is performed iteratively to obtain better estimates.

4.4 Performance Results

In this subsection, we present the performance of some of the channel estimation methods presented in the previous subsections. The OTFS system considered has a carrier frequency of 4 GHz, a subcarrier spacing of 15 kHz, and a DD grid with $M = N = 32$. A multipath channel with $P = 5$ paths, exponential power delay profile, and delay-Doppler profile shown in Table 3 are considered. Fig. 17 shows the mean squared error (MSE) performance as a function of pilot SNR for 1) OMP, 2) impulse based estimation, and 3) embedded pilot based estimation. A pilot frame with i.i.d Gaussian random sequences occupying the entire DD grid is used for

▼ Table 3. Delay-Doppler profile for Figures 17 and 18

Path (i)	1	2	3	4	5
Delay τ_i	$\frac{1}{M\Delta f}$	$\frac{2}{M\Delta f}$	$\frac{3}{M\Delta f}$	$\frac{4}{M\Delta f}$	$\frac{5}{M\Delta f}$
Doppler ν_i	0	$\frac{1}{NT}$	$\frac{2}{NT}$	$\frac{3}{NT}$	$\frac{4}{NT}$



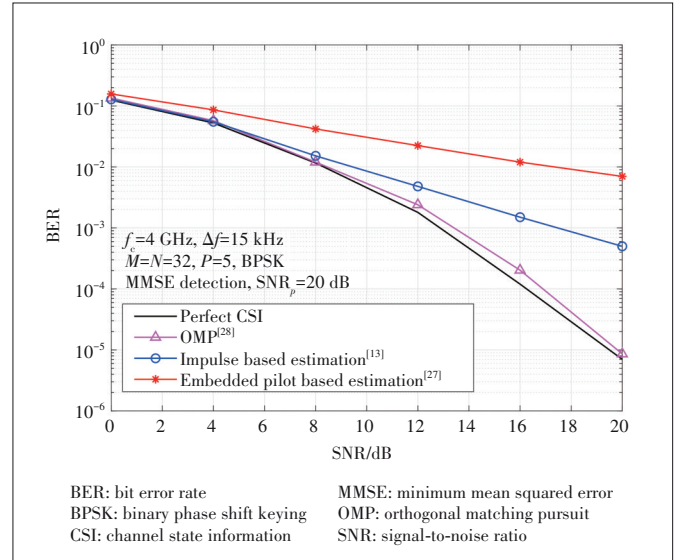
▲ Figure 17. Mean squared error performance of delay-Doppler (DD) channel estimation methods

OMP based channel estimation. A pilot frame with an impulse at location $(k_p, l_p) = (15, 15)$ and zeros elsewhere is considered for impulse based channel estimation. An embedded frame is used for embedded pilot based channel estimation, with impulse as a pilot at location $(k_p, l_p) = (15, 15)$, guard symbols in the locations $7 \leq k \leq 23, 10 \leq l \leq 20$, and data symbols elsewhere.

It can be seen from Fig. 17 that the OMP algorithm gives the channel estimate with small MSE, which is in the order of 10^{-3} for a pilot SNR of 15 dB. Impulse based channel estimation scheme is simpler but its MSE is high. The MSE of the embedded pilot based channel estimation is also high. Fig. 18 shows the BER performance of these estimation methods using MMSE detection as a function of data SNR for a pilot SNR of 20 dB. BPSK modulation is used. The BER performance of OMP based channel estimation is close to the performance using perfect channel knowledge. Impulse based estimation performance is inferior compared to OMP performance but is superior compared to that of embedded pilot based estimation. Embedded pilot based estimation can be used with high pilot SNRs to achieve good BER performance and higher throughput.

5 Conclusions

OTFS modulation is regarded as an attractive physical layer waveform for future wireless systems. It has demonstrated ro-



▲ Figure 18. BER performance with estimated delay-Doppler (DD) channel at pilot SNR of 20 dB

bust performance in high-Doppler scenarios which are expected in emerging standards. In this paper, we presented an overview of the state-of-the-art approaches in OTFS signal detection and DD channel estimation. We classified the detection approaches as low-complexity linear approach, approximate MAP approach, and DNN approach. Low complexities possible in the linear approach due to the structure of the channel matrix make it attractive for practical implementations. The iterative MAP approach (e.g., message passing) is known for its good performance at low complexities. DNN approach is emerging with good promise particularly when there are model deviations that are typical in practice. In the DD channel estimation space, we highlighted approaches based on exclusive pilot frames, embedded pilot frames, and superimposed pilot frames. More research in OTFS transceiver designs using the DNN approach can be pursued as future work.

References

- [1] HADANI R, RAKIB S, TSATSANIS M, et al. Orthogonal time frequency space modulation [C]//IEEE Wireless Communications and Networking Conference (WCNC). San Francisco, USA: IEEE, 2017: 1 - 6. DOI: 10.1109/WCNC.2017.7925924
- [2] HADANI R, MONK A. OTFS: a new generation of modulation addressing the challenges of 5G [EB/OL]. (2018-02-07)[2021-09-25]. <https://arxiv.org/ftp/arxiv/papers/1802/1802.02623.pdf>
- [3] HADANI R, RAKIB S, TSATSANIS M, et al. Orthogonal time frequency space modulation [EB/OL]. (2018-08-01)[2021-09-25]. <https://arxiv.org/abs/1808.00519v1>
- [4] HADANI R, RAKIB S, MOLISCH A F, et al. Orthogonal time frequency

- space (OTFS) modulation for millimeter-wave communications systems [C]// 2017 IEEE MTT-S International Microwave Symposium (IMS). Honolulu, USA: IEEE, 2017: 681 – 683. DOI: 10.1109/MWSYM.2017.8058662
- [5] WIFFEN F, SAYER L, BOCUS M Z, et al. Comparison of OTFS and OFDM in ray launched sub-6 GHz and mmWave line-of-sight mobility channels [C]// IEEE 29th Annual International Symposium on Personal, Indoor and Mobile Radio Communications (PIMRC). Bologna, Italy: IEEE, 2018: 73 – 79. DOI: 10.1109/PIMRC.2018.8580850
- [6] RAMACHANDRAN M K, SURABHI G D, CHOCKALINGAM A. OTFS: a new modulation scheme for high-mobility use cases [J]. *Journal of the Indian institute of science*, 2020, 100(2): 315 – 336. DOI: 10.1007/s41745-020-00167-4
- [7] MOHAMMED S K. Derivation of OTFS modulation from first principles [J]. *IEEE transactions on vehicular technology*, 2021, 70(8): 7619 – 7636. DOI: 10.1109/TVT.2021.3069913
- [8] MURALI K R, CHOCKALINGAM A. On OTFS modulation for high-Doppler fading channels [C]// *Information Theory and Applications Workshop (ITA)*. San Diego, USA: IEEE, 2018: 1 – 10. DOI: 10.1109/ITA.2018.8503182
- [9] SURABHI G D, AUGUSTINE R M, CHOCKALINGAM A. On the diversity of uncoded OTFS modulation in doubly-dispersive channels [J]. *IEEE transactions on wireless communications*, 2019, 18(6): 3049 – 3063. DOI: 10.1109/TWC.2019.2909205
- [10] GUNTURU A, GODALA A R, SAHOO A K, et al. Performance analysis of OTFS waveform for 5G NR mmWave communication system [C]// *IEEE Wireless Communications and Networking Conference (WCNC)*. Nanjing, China: IEEE, 2021: 1 – 6. DOI: 10.1109/WCNC49053.2021.9417346
- [11] RAVITEJA P, PHAN K T, HONG Y, et al. Interference cancellation and iterative detection for orthogonal time frequency space modulation [J]. *IEEE transactions on wireless communications*, 2018, 17(10): 6501 – 6515. DOI: 10.1109/TWC.2018.2860011
- [12] THAJ T, VITERBO E. Low complexity iterative rake detector for orthogonal time frequency space modulation [C]// *IEEE Wireless Communications and Networking Conference (WCNC)*. Seoul, Korea (South): IEEE, 2020: 1 – 6. DOI: 10.1109/WCNC45663.2020.9120526
- [13] KOLLENGODE RAMACHANDRAN M, CHOCKALINGAM A. MIMO-OTFS in high-Doppler fading channels: signal detection and channel estimation [C]// *IEEE Global Communications Conference (GLOBECOM)*. Abu Dhabi, United Arab Emirates: IEEE, 2018: 206 – 212. DOI: 10.1109/GLOBECOM.2018.8647394
- [14] LI L J, LIANG Y, FAN P Z, et al. Low complexity detection algorithms for OTFS under rapidly time-varying channel [C]// *IEEE 89th Vehicular Technology Conference (VTC2019-Spring)*. Kuala Lumpur, Malaysia: IEEE, 2019: 1 – 5. DOI: 10.1109/VTCSpring.2019.8746420
- [15] ZHANG H J, ZHANG T T. A low-complexity message passing detector for OTFS modulation with probability clipping [J]. *IEEE wireless communications letters*, 2021, 10(6): 1271 – 1275. DOI: 10.1109/LWC.2021.3063904
- [16] LI S Y, YUAN W J, WEI Z Q, et al. Hybrid MAP and PIC detection for OTFS modulation [J]. *IEEE transactions on vehicular technology*, 2021, 70(7): 7193 – 7198. DOI: 10.1109/tvt.2021.3083181
- [17] XIANG L P, LIU Y S, YANG L L, et al. Gaussian approximate message passing detection of orthogonal time frequency space modulation [J]. *IEEE transactions on vehicular technology*, 2021, 70(10): 10999 – 11004. DOI: 10.1109/TVT.2021.3102673
- [18] NAIKOTI A, CHOCKALINGAM A. Low-complexity delay-Doppler symbol DNN for OTFS signal detection [C]// *IEEE 93rd Vehicular Technology Conference (VTC2021-Spring)*. Helsinki, Finland: IEEE, 2021: 1 – 6. DOI: 10.1109/VTC2021-Spring51267.2021.9448630
- [19] ENKU Y K, BAI B M, WAN F, et al. Two-dimensional convolutional neural network-based signal detection for OTFS systems [J]. *IEEE wireless communications letters*, 2021, 10(11): 2514 – 2518. DOI: 10.1109/LWC.2021.3106039
- [20] YUAN W J, WEI Z Q, YUAN J H, et al. A simple variational Bayes detector for orthogonal time frequency space (OTFS) modulation [J]. *IEEE transactions on vehicular technology*, 2020, 69(7): 7976 – 7980. DOI: 10.1109/TVT.2020.2991443
- [21] SURABHI G D, CHOCKALINGAM A. Low-complexity linear equalization for OTFS modulation [J]. *IEEE communications letters*, 2020, 24(2): 330 – 334. DOI: 10.1109/LCOMM.2019.2956709
- [22] SURABHI G D, CHOCKALINGAM A. Low-complexity linear equalization for 2x2 MIMO-OTFS signals [C]// *IEEE 21st International Workshop on Signal Processing Advances in Wireless Communications (SPAWC)*. Atlanta, USA: IEEE, 2020: 1 – 5. DOI: 10.1109/SPAWC48557.2020.9154292
- [23] TIWARI S, DAS S S, RANGAMGARI V. Low complexity LMMSE Receiver for OTFS [J]. *IEEE communications letters*, 2019, 23(12): 2205 – 2209. DOI: 10.1109/LCOMM.2019.2945564
- [24] LONG F, NIU K, DONG C, et al. Low complexity iterative LMMSE-PIC equalizer for OTFS [C]// *IEEE International Conference on Communications (ICC)*. Shanghai, China: IEEE, 2019: 1 – 6. DOI: 10.1109/ICC.2019.8761635
- [25] JING L Y, WANG H, HE C B, et al. Two dimensional adaptive multichannel decision feedback equalization for OTFS system [J]. *IEEE communications letters*, 2021, 25(3): 840 – 844. DOI: 10.1109/LCOMM.2020.3039982
- [26] PANDEY B C, MOHAMMED S K, RAVITEJA P, et al. Low complexity precoding and detection in multi-user massive MIMO OTFS downlink [J]. *IEEE transactions on vehicular technology*, 2021, 70(5): 4389 – 4405. DOI: 10.1109/TVT.2021.3061694
- [27] RAVITEJA P, PHAN K T, HONG Y. Embedded pilot-aided channel estimation for OTFS in delay – Doppler channels [J]. *IEEE transactions on vehicular technology*, 2019, 68(5): 4906 – 4917. DOI: 10.1109/TVT.2019.2906357
- [28] RASHEED O K, SURABHI G D, CHOCKALINGAM A. Sparse delay-Doppler channel estimation in rapidly time-varying channels for multiuser OTFS on the uplink [C]// *IEEE 91st Vehicular Technology Conference (VTC2020-Spring)*. Antwerp, Belgium: IEEE, 2020: 1 – 5. DOI: 10.1109/VTC2020-Spring48590.2020.9128497
- [29] ZHAO L, GAO W J, GUO W B. Sparse Bayesian learning of delay-Doppler channel for OTFS system [J]. *IEEE communications letters*, 2020, 24(12): 2766 – 2769. DOI: 10.1109/LCOMM.2020.3021120
- [30] SRIVASTAVA S, SINGH R K, JAGANNATHAM A K, et al. Bayesian learning aided sparse channel estimation for orthogonal time frequency space modulated systems [J]. *IEEE transactions on vehicular technology*, 70(8): 8343 – 8348. DOI: 10.1109/TCOMM.2021.3123354
- [31] SHEN W Q, DAI L L, HAN S F, et al. Channel estimation for orthogonal time frequency space (OTFS) massive MIMO [C]// *IEEE International Conference on Communications (ICC)*. Shanghai, China: IEEE, 2019: 1 – 6. DOI: 10.1109/ICC.2019.8761362
- [32] ZHAO H, KANG Z Q, WANG H. A novel channel estimation scheme for OTFS [C]// *IEEE 20th International Conference on Communication Technology (ICCT)*. Nanning, China: IEEE, 2020: 12 – 16. DOI: 10.1109/ICCT50939.2020.9295699
- [33] BOMFIN R, CHAFII M, NIMR A, et al. Channel estimation for MIMO space time coded OTFS under doubly selective channels [C]// *IEEE International Conference on Communications Workshops (ICC Workshops)*. Montreal, Canada: IEEE, 2021: 1 – 6. DOI: 10.1109/ICCWshops50388.2021.9473618
- [34] LIU F, YUAN Z D, GUO Q H, et al. Message passing based structured sparse signal recovery for estimation of OTFS channels with fractional Doppler shifts [J]. *IEEE transactions on wireless communications*, 2021, early access. DOI: 10.1109/TWC.2021.3087501
- [35] MISHRA H B, SINGH P, PRASAD A K, et al. OTFS channel estimation and data detection designs with superimposed pilots [J]. *IEEE transactions on wireless communications*, 2021, early access. DOI: 10.1109/TWC.2021.3110659
- [36] YUAN W J, LI S Y, WEI Z Q, et al. Data-aided channel estimation for OTFS systems with a superimposed pilot and data transmission scheme [J]. *IEEE wireless communications letters*, 2021, 10(9): 1954 – 1958. DOI: 10.1109/LWC.2021.3088836
- [37] YUAN Z D, LIU F, YUAN W J, et al. Iterative detection for orthogonal time frequency space modulation with unitary approximate message passing [EB/OL]. (2021-02-16)[2021-09-25]. <https://arxiv.org/abs/2008.06688v3>
- [38] LI L, WEI H, HUANG Y, et al. A simple two-stage equalizer with simplified orthogonal time frequency space modulation over rapidly time-varying channels [EB/OL]. (2017-09-08)[2021-09-25]. <https://arxiv.org/abs/1709.02505>
- [39] ZEMEN T, HOFER M, LOESCHENBRAND D. Low-complexity equalization for orthogonal time and frequency signaling (OTFS) [EB/OL]. (2017-10-26)[2021-09-25]. <https://arxiv.org/pdf/1710.09916v1.pdf>
- [40] THAJ T, VITERBO E. Low complexity iterative rake decision feedback equalizer for zero-padded OTFS systems [J]. *IEEE transactions on vehicular technology*, 2020, 69(12): 15606 – 15622. DOI: 10.1109/TVT.2020.3044276

- [41] LI S Y, YUAN W J, WEI Z Q, et al. Cross domain iterative detection for orthogonal time frequency space modulation [EB/OL]. (2021-01-11)[2021-09-25]. <https://arxiv.org/abs/2101.03822v1>
- [42] XU W J, ZOU T T, GAO H, et al. Low-complexity linear equalization for OTFS systems with rectangular waveforms [EB/OL]. (2019-11-19)[2021-09-25]. <https://arxiv.org/abs/1911.08133v1>
- [43] LIU Y S, ZHANG S, GAO F F, et al. Uplink-aided high mobility downlink channel estimation over massive MIMO-OTFS system [J]. *IEEE journal on selected areas in communications*, 2020, 38(9): 1994 – 2009. DOI: 10.1109/JSAC.2020.3000884
- [44] DAS S S, RANGAMGARI V, TIWARI S, et al. Time domain channel estimation and equalization of CP-OTFS under multiple fractional Dopplers and residual synchronization errors [J]. *IEEE Access*, 2021, 9: 10561 – 10576. DOI: 10.1109/ACCESS.2020.3046487
- [45] YAN H, WANG M. A low complexity channel estimation scheme for orthogonal time frequency space (OTFS) system with synchronization errors [C]// *IEEE 6th International Conference on Computer and Communication Systems (ICCCS)*. Chengdu, China: IEEE, 2021: 576 – 581. DOI: 10.1109/ICCCS52626.2021.9449209
- [46] WU X D, MA S D, YANG X. Tensor-based low-complexity channel estimation for mmWave massive MIMO-OTFS systems [J]. *Journal of communications and information networks*, 2020, 5(3): 324 – 334. DOI: 10.23919/JCIN.2020.9200896
- [47] KUMAR SINGH V, FLANAGAN M F, CARDIFF B. Maximum likelihood channel path detection and MMSE channel estimation in OTFS systems [C]// *IEEE 92nd Vehicular Technology Conference (VTC2020-Fall)*. Victoria, Canada: IEEE, 2020: 1 – 5. DOI: 10.1109/VTC2020-Fall49728.2020.9348590
- [48] SHI D, WANG W J, YOU L, et al. Deterministic pilot design and channel estimation for downlink massive MIMO-OTFS systems in presence of the fractional Doppler [J]. *IEEE transactions on wireless communications*, 2021, early access. DOI: 10.1109/TWC.2021.3081164
- [49] ZHANG M C, WANG F G, YUAN X J, et al. 2D structured turbo compressed sensing for channel estimation in OTFS systems [C]// *IEEE International Conference on Communication Systems (ICCS)*. Chengdu, China: IEEE, 2018: 45 – 49. DOI: 10.1109/ICCS.2018.8689234
- [50] HASHIMOTO N, OSAWA N, YAMAZAKI K, et al. Channel estimation and equalization for CP-OFDM-based OTFS in fractional Doppler channels [C]// *IEEE International Conference on Communications Workshops (ICC Workshops)*. Montreal, Canada: IEEE, 2021: 1 – 7. DOI: 10.1109/ICCWorkshops50388.2021.9473532
- [51] QU H Y, LIU G H, ZHANG L, et al. Low-dimensional subspace estimation of continuous-Doppler-spread channel in OTFS systems [J]. *IEEE transactions on communications*, 2021, 69(7): 4717 – 4731. DOI: 10.1109/TCOMM.2021.3072744
- [52] ABDELGADER A M S, WU L N. The physical layer of the IEEE 802.11p WAVE communication standard: the specifications and challenges [C]// *World Congress on Engineering and Computer Science 2014*. San Francisco, USA: IAENG, 2014
- [53] KRUSEVAC S, RAPAJIC P, KENNEDY R A. Channel capacity estimation for MIMO systems with correlated noise [C]// *IEEE Global Telecommunications Conference*. St. Louis, USA: IEEE, 2005: 2812 – 2816. DOI: 10.1109/GLOCOM.2005.1578272

Biographies

Ashwitha NAIKOTI (ashwithan@iisc.ac.in) received the B.Tech. degree in electronics and communication engineering from the National Institute of Technology, Warangal, India in 2017. She is currently pursuing M. Tech (Research) degree with the Department of Electrical Communication Engineering, Indian Institute of Science (IISc), Bengaluru, India. She was with the Center for Development of Telematics, Bengaluru, as a Research Engineer from 2017 to 2019. Her current research interests include orthogonal time frequency space modulation and transceiver design using neural networks.

Ananthanarayanan CHOCKALINGAM received the Ph. D. degree in electrical communication engineering (ECE) from the Indian Institute of Science (IISc), Bangalore, India. He was a post-doctoral fellow and an assistant project scientist with the Department of Electrical and Computer Engineering, University of California, San Diego, USA. He was with Qualcomm, Inc., San Diego, USA as a Staff Engineer/Manager. Currently, he is a professor with the Department of ECE, IISc, Bangalore. He served as an associate editor for the *IEEE Transactions on Vehicular Technology*, an editor for the *IEEE Transactions on Wireless Communications*, and a guest editor for the *IEEE Journal on Selected Areas in Communications* and the *IEEE Journal of Selected Topics in Signal Processing*. He is an author of the book *Large MIMO Systems* published by Cambridge University Press.